

### 3-(4-Aroyl-1-methyl-1*H*-2-pyrrolyl)-*N*-hydroxy-2-alkylamides as a New Class of Synthetic Histone Deacetylase Inhibitors. 1. Design, Synthesis, Biological Evaluation, and Binding Mode Studies Performed through Three Different Docking Procedures

Antonello Mai,<sup>\*,§</sup> Silvio Massa,<sup>‡</sup> Rino Ragno,<sup>\*,#</sup> Ilaria Cerbara,<sup>§</sup> Florian Jesacher,<sup>‡</sup> Peter Loidl,<sup>‡</sup> and Gerald Brosch<sup>\*,‡</sup>

Dipartimento di Studi Farmaceutici, Università degli Studi di Roma "La Sapienza", P. le A. Moro 5, 00185 Roma, Italy, Dipartimento Farmaco Chimico Tecnologico, Università degli Studi di Siena, via A. Moro, 53100 Siena, Italy, Dipartimento di Studi di Chimica e Tecnologia delle Sostanze Biologicamente Attive, Università degli Studi di Roma "La Sapienza", P. le A. Moro 5, 00185 Roma, Italy, and Department of Microbiology, University of Innsbruck, Medical School, Fritz-Pregl-Strasse 3, 6020 Innsbruck, Austria

Received October 14, 2002

Recently we reported a novel series of hydroxamates, called 3-(4-*aroyl*-1*H*-2-pyrrolyl)-*N*-hydroxy-2-propenamides (APHAs), acting as HDAC inhibitors (Massa, S.; et al. *J. Med. Chem.* **2001**, *44*, 2069–2072). Among them, 3-(4-benzoyl-1-methyl-1*H*-2-pyrrolyl)-*N*-hydroxy-2-propenamide **1** was chosen as lead compound, and its binding mode into the modeled HDAC1 catalytic core together with its histone hyperacetylation, antiproliferative, and cytodifferentiating properties in cell-based assays were investigated (Mai, A.; et al. *J. Med. Chem.* **2002**, *45*, 1778–1784). Here we report the results of some chemical manipulations performed on (i) the *aroyl* portion at the C<sub>4</sub>-pyrrole position, (ii) the N<sub>1</sub>-pyrrole substituent, and (iii) the hydroxamate moiety of **1** to determine structure–activity relationships and to improve enzyme inhibitory activity of APHAs. In the **1** structure, pyrrole N<sub>1</sub>-substitution with groups larger than methyl gave a reduction in HDAC inhibiting activity, and replacement of hydroxamate function with various non-hydroxamate, metal ion-complexing groups yielded poorly active or totally inactive compounds. On the contrary, proper substitution at the C<sub>4</sub>-position favorably affected enzyme inhibiting potency, leading to **8** (IC<sub>50</sub> = 0.1 μM) and **9** (IC<sub>50</sub> = 1.0 μM) which were 38- and 3.8-fold more potent than **1** in in vitro anti-HD2 assay. Against mouse HDAC1, **8** showed an IC<sub>50</sub> = 0.5 μM (IC<sub>50</sub> of **1** = 4.9 μM), and also in cell-based assay, **8** was endowed with higher histone hyperacetylating activity than **1**, although it was less potent than TSA and SAHA. Such enhancement of inhibitory activity can be explained by the higher flexibility of the pyrrole C<sub>4</sub>-substituent of **8** which accounts for a considerably better fitting into the HDAC1 pocket and a more favorable enthalpy ligand receptor energy compared to **1**. The enhanced fit allows a closer positioning of **8** hydroxamate moiety to the zinc ion. These findings were supported by extensive docking studies (SAD, DOCK, and Autodock) performed on both APHAs and reference drugs (TSA and SAHA).

#### Introduction

Chromatin is a nuclear macromolecular complex containing DNA, histones, and nonhistone proteins.<sup>1</sup> The basic functional unit of chromatin is the nucleosome, consisting of DNA wrapped around a histone octamer of pairs of H2A, H2B, H3, and H4 proteins.<sup>2,3</sup>

Dynamic changes in nucleosomal packaging of DNA define distinct levels of chromatin organization. Local remodeling of higher-order chromatin structure plays a key role in the regulation of gene expression affecting proper cell function, differentiation, and proliferation.

One of the key steps in the regulation of expression of target genes is the posttranslational modification of the N-terminal tails of core histones by acetylation.<sup>4–6</sup> Acetylation of Lys residues, predominantly in histones H3 and H4, is catalyzed by enzymes with histone acetyltransferase (HAT) activity. Such acetylation is associated with relaxation of DNA wrapped around the core histones and produces transcriptionally active chromatin regions. On the other hand, histone deacetylase (HDAC) enzymes remove acetyl groups from  $\epsilon$ -*N*-acetyl-lysine histone tails and restore a positive charge to the Lys residues. Such chemical modifications result in a tightening of nucleosome structure and gene silencing.<sup>7–10</sup>

Aberrant acetylation of histone tails emerging from HAT mutations or abnormal recruitment of HDACs has been clearly linked to carcinogenesis. Rubinstein–Taybi syndrome,<sup>11–14</sup> acute promyelocytic leukemia (APL),<sup>15–18</sup> acute myelogenous leukemia (AML) involving AML1-ETO fusion protein,<sup>19–22</sup> non-Hodgkin's lymphoma with

\* To whom correspondence should be addressed. A.M., Tel.: +396-4991-3392; Fax: +396491491; e-mail: antonello.mai@uniroma1.it. (Molecular Modeling) R.R., Tel.: +396-4991-3152. Fax: +396491491. e-mail: rino.ragno@uniroma1.it. (Biology) G.B., Tel.: 0512-507-3608; Fax: 0512-507-2866; e-mail: gerald.brosch@uibk.ac.at.

<sup>§</sup> Dipartimento di Studi Farmaceutici, Università degli Studi di Roma "La Sapienza".

<sup>‡</sup> Università degli Studi di Siena.

<sup>#</sup> Dipartimento di Studi di Chimica e Tecnologia delle Sostanze Biologicamente Attive, Università degli Studi di Roma "La Sapienza".

<sup>‡</sup> University of Innsbruck.

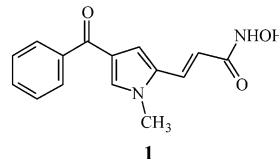
overexpression of the BCL-6 oncogene repressor,<sup>23</sup> and some colorectal and gastric carcinomas<sup>24</sup> are examples of cancer diseases associated with an upset of biological HAT/HDAC balance. Although the molecular basis of many neoplasias is still largely unexplored, it has been widely established that inappropriate HDAC-mediated transcriptional repression represents a common molecular mechanism used by oncoproteins to produce alterations in chromatin structure and blockage of normal cell differentiation. From these data, compounds able to inhibit HDAC activity are expected to reverse repression and to induce reexpression of differentiation-inducing genes.<sup>25–29</sup>

A number of natural or synthetic compounds have been so far reported exhibiting HDAC inhibiting activity. Among them, trichostatin A (TSA),<sup>30</sup> cyclic tetrapeptide trapoxin (TPX),<sup>31</sup> HC toxin,<sup>32</sup> apicidin,<sup>33</sup> depsipeptide FK-228,<sup>34</sup> and sodium butyrate<sup>35</sup> are examples of natural substances endowed with anti-HDAC activity. Synthetic HDAC inhibitors can be represented by sodium phenylbutyrate,<sup>36</sup> sodium valproate,<sup>37,38</sup> suberoylanilide hydroxamic acid (SAHA),<sup>39</sup> straight chain TSA- and SAHA-like analogues,<sup>40–42</sup> 1,4-cyclohexylene- and 1,4-phenylene-*N*-hydroxycarboxamides,<sup>43</sup> scrip-taid,<sup>44</sup> oxamflatin<sup>45</sup> and related compounds,<sup>46</sup> cyclic hydroxamic acid-containing peptides (CHAPs),<sup>47,48</sup> and the benzamide MS-275.<sup>49,50</sup>

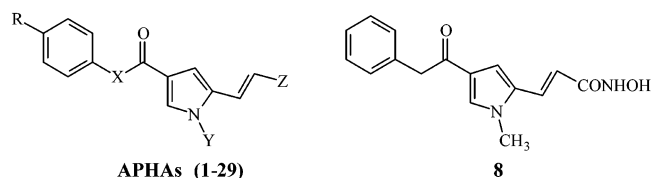
Many of these compounds have been shown to have potent antitumor effect in vivo in tumor-bearing animals, and some of them are currently in phase I or phase I/II clinical trials.<sup>29</sup> However, in some cases their potential for clinical drug development could be limited by low potency and lack of selectivity (butyrates and analogues), cytotoxicity (TSA, CHAPs, MS-275), low solubility in the aqueous vehicle (TSA), and/or low stability in cell culture (TSA, trapoxin).<sup>51</sup>

Recently, we reported a novel series of hydroxamate compounds, namely, 3-(4-aroil-1*H*-2-pyrrolyl)-*N*-hydroxy-2-propenamides (APHAs), acting as HDAC inhibitors.<sup>52,53</sup> The X-ray crystal structure of the catalytic core of an archaeobacterial HDAC homologue (histone deacetylase-like protein, HDLP), reported in 1999 by Finnin et al.,<sup>54</sup> revealed the mode by which the hydroxamic acid-based HDAC inhibitors TSA and SAHA bind to the pocket of the catalytic site of the enzyme. These data prompted us to perform three-dimensional (3D) structure-based design and molecular modeling studies on previously reported<sup>55,56</sup> and newly synthesized aroil-pyrrole-hydroxyamides, with the aim to explore their capability to bind the deacetylase catalytic core. An extended VALIDATE QSAR/scoring function hybrid model<sup>57</sup> predicted the  $pK_i$  values of such derivatives complexed with HDLP in the low (or sub-) micromolar range.<sup>52</sup> Subsequent enzyme-based assay against maize histone deacetylase HD2 performed on pyrrole compounds revealed  $IC_{50}$  values at low micromolar concentrations in good agreement with the corresponding predicted  $pK_i$  values.<sup>52</sup> The binding mode of 3-(4-benzoyl-1-methyl-1*H*-2-pyrrolyl)-*N*-hydroxy-2-propenamide **1**, chosen as APHA lead compound, into the HDAC1 (RPD3 homologue) catalytic core was further investigated by modeling the HDAC1 X-ray coordinates from those of HDLP.<sup>53</sup> The modeled HDAC1/**1** complex, subjected to the VALIDATE model, afforded lower absolute error of prediction (AEP)

than that observed for the corresponding HDLP/1 complex.<sup>53</sup> In in vivo assays, **1** induced histone hyperacetylation on mouse A20 cells and was endowed with antiproliferative and cellular differentiation activities in murine erytroleukemic cells.<sup>53</sup>



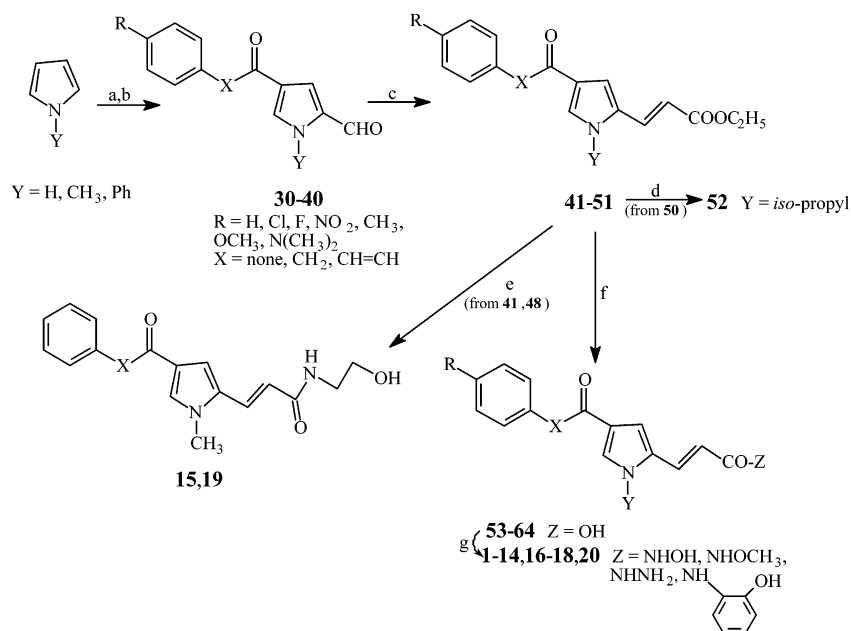
Prompted by these results, in the chemical skeleton of compound **1** we identified several structural features to subject to chemical modifications for determining structure–activity relationships (SARs) and for improving HDAC inhibitory activity of APHA analogues. Particularly, (i) the aroil portion at the C<sub>4</sub>-pyrrole position, (ii) the N<sub>1</sub>-pyrrole substituent, and (iii) the hydroxamate moiety of **1**, were chosen for chemical modifications. Novel pyrrole derivatives **1–29** bearing several aroil groups at C<sub>4</sub>-position, hydrogen, methyl, isopropyl, or phenyl substituents at the N<sub>1</sub>-position, and various hydroxamate or non-hydroxamate, metal ion-complexing moieties on the unsaturated chain linked at the C<sub>2</sub>-position of the pyrrole ring, were synthesized and tested to determine their HDAC inhibitory activity in vitro. 3-(1-Methyl-4-phenylacetyl-1*H*-2-pyrrolyl)-*N*-hydroxy-2-propenamide **8**, the most potent compound resulting from such chemical manipulations, was further investigated about its binding mode into the HDAC1 catalytic core and its in vivo histone hyperacetylating activity on mouse A20 cells.



R = H, Cl, F, NO<sub>2</sub>, CH<sub>3</sub>, OCH<sub>3</sub>, N(CH<sub>3</sub>)<sub>2</sub>,  
X = none, CH<sub>2</sub>, CH=CH  
Y = H, CH<sub>3</sub>, CH(CH<sub>3</sub>)<sub>2</sub>, Ph  
Z = CONH<sub>2</sub>, CONHCH<sub>3</sub>, CONHNH<sub>2</sub>, CONH(CH<sub>2</sub>)<sub>2</sub>OH,  
CONH-(2'-OH)-Ph, PO(OC<sub>2</sub>H<sub>5</sub>)<sub>2</sub>OH, C5-barbituric acid moiety,  
C5-thiobarbituric acid moiety, CN, C=NH(NH<sub>2</sub>)

## Chemistry

Hydroxamic acids **1–12** (Scheme 1) were synthesized from the corresponding pyrrolepropenoic acids **53–64** and hydroxylamine via ethoxycarbonyl anhydrides. *O*-Methylhydroxamates (**13**, **17**), hydrazides (**14**, **18**), and 2'-hydroxyanilides (**16**, **20**) were prepared in a similar manner from the propenoic acids **53**, **60** using *O*-methylhydroxylamine, hydrazine, and 2-hydroxyaniline instead of hydroxylamine. 2-Hydroxyethylamides (**15**, **19**) were obtained by heating ethyl pyrrolepropenoates **41**, **48** with 2-hydroxyethylamine. The propenoic acids **53–63** were readily obtained by a Wittig–Horner reaction between 4-aroil-1*H*-pyrrole-2-carboxaldehydes (**30–40**) and triethyl phosphonoacetate in the presence of potassium carbonate, followed by alkaline hydrolysis of the resulting ethyl pyrrolepropenoates (**41–51**). 3-[4-Benzoyl-1-(1-methylethyl)-1*H*-2-pyrrolyl]propenoic acid **64** was prepared by alkylation of ethyl N<sub>1</sub>-unsubstituted pyrrolepropenoate **50** and subsequent alkaline hydroly-

Scheme 1<sup>a</sup>

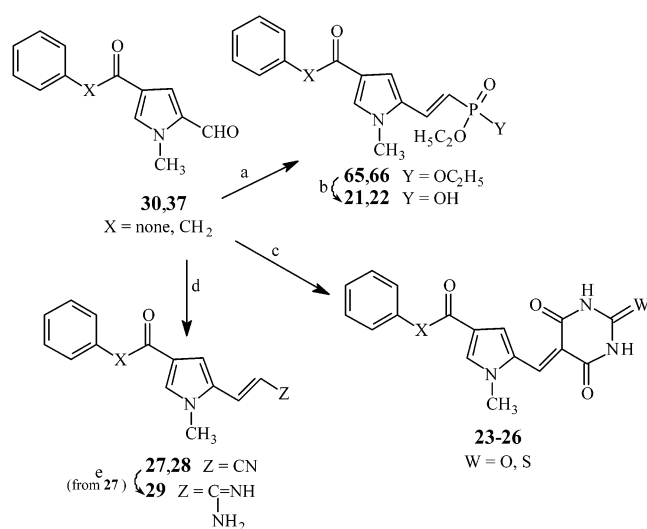
<sup>a</sup> (a) (COCl)<sub>2</sub>, DMF, dichloroethane, 0 °C; (b) (1) R-Ph-X-COCl, AlCl<sub>3</sub>, rt; (2) NaOH 50%, rt; (c) (C<sub>2</sub>H<sub>5</sub>O)<sub>2</sub>OPCH<sub>2</sub>COOC<sub>2</sub>H<sub>5</sub>, K<sub>2</sub>CO<sub>3</sub>, C<sub>2</sub>H<sub>5</sub>OH, 80 °C; (d) 2-iodopropane, K<sub>2</sub>CO<sub>3</sub>, DMF, 90 °C; (e) NH<sub>2</sub>CH<sub>2</sub>CH<sub>2</sub>OH, 140 °C; (f) KOH, C<sub>2</sub>H<sub>5</sub>OH, H<sub>2</sub>O, 70 °C; (g) (1) ClCOOC<sub>2</sub>H<sub>5</sub>, (C<sub>2</sub>H<sub>5</sub>)<sub>3</sub>N, THF, 0 °C; (2) NH<sub>2</sub>OH, or NH<sub>2</sub>OCH<sub>3</sub>, or NHNH<sub>2</sub>, or NH<sub>2</sub>-(2'-OH)-Ph, rt.

sis of the obtained ester **52**. The pyrrolealdehydes **30**–**40**, key intermediates for the synthesis of title compounds, were prepared by acylation of the Vilmeier–Haack intermediates formed from pyrrole, 1-methylpyrrole, or 1-phenylpyrrole, and a mixture of *N,N*-dimethylformamide and oxalyl chloride, with the proper aroyl chloride under Friedel–Crafts conditions (Scheme 1).

Further compounds (Scheme 2) were prepared by reacting the pyrrolealdehydes **30**, **37** with tetraethyl methylenediphosphonate or diethyl cyanomethylphosphonate under Wittig–Horner conditions. In the first reaction two diethyl pyrroleethenylphosphonates (**65**, **66**) were obtained, which were in turn transformed into the corresponding monophosphonic acids **21**, **22** by alkaline hydrolysis. The latter reaction yielded the pyrrolepropenenitriles **27**, **28**; among them, **27** was converted into the related pyrrolepropenylamidine **29** with trimethylaluminum and ammonium chloride according to the Garigipati procedure.<sup>58</sup> Finally, condensation of **30**, **37** with barbituric and thiobarbituric acids gave the pyrroleethenyl(thio)barbiturates **23**–**26** (Scheme 2).

Chemical and physical data of compounds **1**–**29** are listed in Table A (see Supporting Information). Chemical and physical data of intermediate compounds **37**–**40**, **48**–**52**, **60**–**66** are listed in Table B (See Supporting Information).

**Biological Evaluation and Structure–Activity Relationship Studies. In Vitro Enzyme Inhibition.** The pyrrole derivatives **1**–**29** were evaluated for their ability to inhibit HDAC activity<sup>59</sup> using maize histone deacetylase HD2 as the enzyme source.<sup>60</sup> HD2 was characterized in detail by us<sup>61,63</sup> and has an *in vitro* enzyme activity comparable to those of HDACs from other sources, such as fungi and vertebrates, using our standard HDAC assay.<sup>59,64</sup> In enzyme inhibition assays, HD2 was 1.3–2.4-fold more sensitive than mouse HDAC1

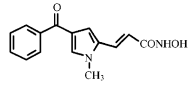
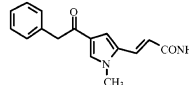
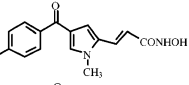
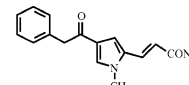
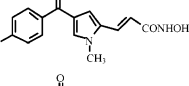
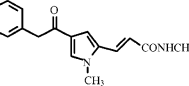
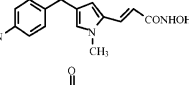
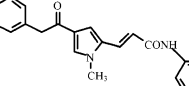
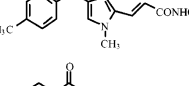
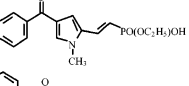
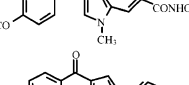
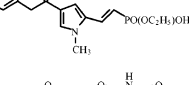
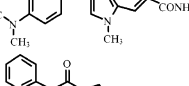
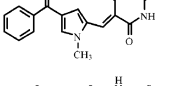
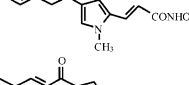
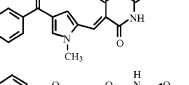
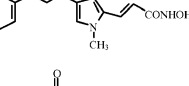
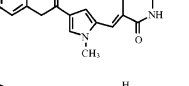
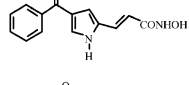
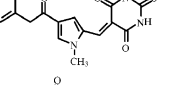
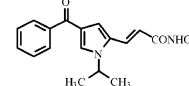
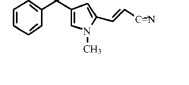
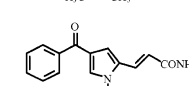
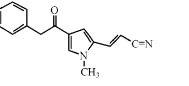
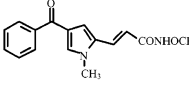
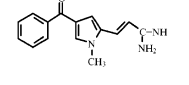
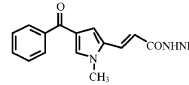
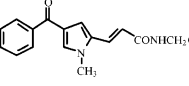
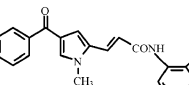
Scheme 2<sup>a</sup>

<sup>a</sup> (a) (C<sub>2</sub>H<sub>5</sub>O)<sub>2</sub>OPCH<sub>2</sub>PO(OC<sub>2</sub>H<sub>5</sub>)<sub>2</sub>, K<sub>2</sub>CO<sub>3</sub>, C<sub>2</sub>H<sub>5</sub>OH, 80 °C; (b) KOH, C<sub>2</sub>H<sub>5</sub>OH, H<sub>2</sub>O, 70 °C; (c) (thio)barbituric acid, H<sub>2</sub>O, C<sub>2</sub>H<sub>5</sub>OH, rt; (d) (C<sub>2</sub>H<sub>5</sub>O)<sub>2</sub>OPCH<sub>2</sub>CN, K<sub>2</sub>CO<sub>3</sub>, C<sub>2</sub>H<sub>5</sub>OH, 80 °C; (e) (1) (CH<sub>3</sub>)<sub>3</sub>Al, NH<sub>4</sub>Cl, *n*-hexane/toluene, from 0 to 80 °C; (2) CH<sub>3</sub>OH, 0 °C.

against three APHA compounds and SAHA and 3.5-fold less sensitive to TSA.<sup>53</sup> Additionally, two short chain fatty acids (sodium butyrate and sodium valproate), two hydroxamic acids (TSA and SAHA), and two cyclic tetrapeptides (trapoxin and HC-toxin) were tested as reference drugs.

The results, expressed as percent of enzyme inhibition at fixed dose and IC<sub>50</sub> (50% inhibitory concentration) values, are reported in Table 1. The effects of some chemical manipulations performed on (i) the aroyl portion at the C<sub>4</sub>-pyrrole position, (ii) the N<sub>1</sub>-pyrrole substituent, and (iii) the hydroxamate moiety of **1** on the biological activity of the compounds are discussed below.

**Table 1.** HDAC Inhibitory Activity of Compounds 1–29<sup>a</sup>

compd	structure	% inhbtn (at fixed dose, $\mu\text{M}$ )	$\text{IC}_{50} \pm \text{SD}$ ( $\mu\text{M}$ )	compd	structure	% inhbtn (at fixed dose, $\mu\text{M}$ )	$\text{IC}_{50} \pm \text{SD}$ ( $\mu\text{M}$ )
1		86 (33)	$3.8 \pm 0.15$	17		NI	-
2		87 (29)	$2.4 \pm 0.07$	18		25.8 (27.1)	ND <sup>c</sup>
3		84 (31)	$3.8 \pm 0.11$	19		NI	-
4		78 (28)	$3.9 \pm 0.19$	20		NI	-
5		86.4 (32)	$1.9 \pm 0.06$	21		NI	-
6		75.2 (30.3)	$2.9 \pm 0.06$	22		NI	-
7		88 (29)	$2.4 \pm 0.07$	23		NI	-
8		96 (29)	$0.1 \pm 0.004$	24		NI	-
9		95 (28)	$1 \pm 0.03$	25		56 (113)	$104 \pm 5.2$
10		91 (30)	$5 \pm 0.15$	26		73 (108)	$85 \pm 3.4$
11		35 (26)	$53 \pm 2.1$	27		69.7 (32.5)	$27.4 \pm 1.6$
12		20.7 (28)	$110 \pm 5.5$	28		NI	-
13		NI <sup>b</sup>	-	29		73.5 (30.4)	$23.3 \pm 0.9$
14		0.2 (33.8)	-			35 (5000)	ND
15		0.9 (30.5)	-				$128 \pm 3.8$
16		NI	-				$0.0072 \pm 0.0002$
							$0.05 \pm 0.0015$
							$0.01 \pm 0.0003$
							$0.11 \pm 0.0044$

<sup>a</sup> Data represent mean values of at least three separate experiments. <sup>b</sup> NI, not inhibition at starting concentration of 30  $\mu\text{M}$ . <sup>c</sup> ND, not determined.

**Aroyl Substitution at the C<sub>4</sub>-Pyrrole Position.** To develop SAR studies on APHA compounds, we prepared a series of pyrrolepropenoic hydroxamates 1–7 showing differently 4'-substituted (4'-H, 4'-chloro, 4'-fluoro, 4'-nitro, 4'-methyl, 4'-methoxy, and 4'-dimethylamino) benzoyl groups at the C<sub>4</sub>-position of the pyrrole ring.

Tested as anti-HDAC agents, these derivatives showed  $\text{IC}_{50}$  values between 1.9 and 3.9  $\mu\text{M}$ , the 4'-chloro-, 4'-methyl-, and 4'-dimethylaminobenzoylpyrrolepropenoic hydroxamates 2, 5, 7 being only just 1.6–2-fold more potent than the unsubstituted 1. Instead, an increase of potency was obtained with the synthesis of 8 and 9,

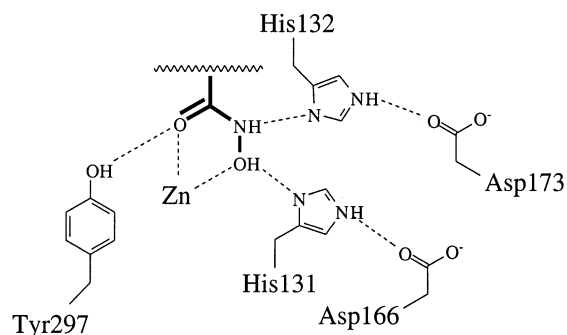


**Figure 1.** Schematic representation of hydroxamate-based inhibitors–HDLP catalytic core interactions

in which the benzene ring of the **1**  $C_4$ -benzoyl moiety is spaced from the carbonyl group through a methylene (**8**) or an ethenyl (**9**) link. Compounds **8** and **9** were 38- and 3.8-fold more effective than **1** in inhibiting HDAC enzyme, respectively.

#### Influence of $N_1$ -Substituent at the Pyrrole Ring.

To study the effect of pyrrole  $N_1$ -substituent on enzyme inhibition we prepared and tested  $N_1$ -H,  $N_1$ -isopropyl, and  $N_1$ -phenyl analogues of **1** (compounds **10**–**12**). The  $N_1$ -H derivative **10** retained the anti-HDAC activity showed by **1** resulting only 1.3-fold less potent than the  $N_1$ -methyl counterpart, while **11** and **12** carrying substituents bulkier than a methyl showed a decrease of inhibitory activity of 14 and 29 times, respectively. These data confirm our observations about the binding mode of **1** into the modeled HDAC1 catalytic core,<sup>53</sup> with the hypothesis of a steric hindrance exerted by pyrrole  $N_1$ -substituent of APHA derivatives into the binding pocket. However, the lack of increasing of activity from  $N_1$ -methyl compound **1** to  $N_1$ -H counterpart **10** can be explained through the display of unfavorable electronic and hydrophilic effects exerted by the NH group into the catalytic pocket. In fact, the calculated logP value for **10** (1.54) is lower than that calculated for **1** (1.85), and this difference accounts for an higher energy that **10** needs to passage by its solvated state to the receptor bound state during the complex formation.

**Replacement of Hydroxamic Acid Moiety.** Crystal structures of HDLP/TSA and HDLP/SAHA complexes revealed that hydroxamic acid-based inhibitors bind the deacetylase core by inserting their aliphatic chains into the HDLP pocket and by making multiple contacts to its tubelike hydrophobic portion.<sup>54</sup> Particularly, their hydroxamic acid group reaches the polar bottom of the pocket, where it coordinates the zinc ion in a bidentate fashion (through CO and OH groups) and also contacts active-site residues (forming two hydrogen-bonds between its NH and OH groups and the two charge-relay systems His131/Asp166 and His132/Asp173, and another one between its CO and the Tyr297 hydroxyl group) (Figure 1). Moreover, hydroxamic acid function replaces the zinc-bound water molecule of the active structure with its OH group.<sup>54</sup>

This mechanism of action underlines the importance of the presence of the CO+NH+OH (or similar, metal ion-complexing structure) for the enzyme inhibiting activity. From these data, we prepared some hydroxamic acid-like derivatives **13**–**20** bearing an *O*-methylhydroxamate (**13**, **17**), hydrazide (**14**, **18**), 2-hydroxyethylamide (**15**, **19**), and 2'-hydroxyanilide (**16**, **20**) moieties

**Table 2.** Maize HD2 and Mouse HDAC1 Inhibitory Activity of **8**

compd	HD2 IC <sub>50</sub> ± SD (μM)	HDAC1 IC <sub>50</sub> ± SD (μM)
<b>8</b>	0.1 ± 0.004	0.51 ± 0.02
<b>1</b> <sup>a</sup>	3.8 ± 0.15	4.9 ± 0.15
TSA <sup>a</sup>	0.007 ± 0.0003	0.002 ± 0.00006
SAHA <sup>a</sup>	0.05 ± 0.0015	0.112 ± 0.0045

**Table 3.** Experimental vs VALIDATE and Autodock Predicted HDAC1 Inhibitory Activities of TSA, SAHA, **1**, and **8**

compd	expt pIC <sub>50</sub>		VALIDATE predicted pK <sub>i</sub>				Autodock predicted pK <sub>i</sub>
	HDAC1	HD2	SAD	DOCK	Autodock		
TSA	8.70	8.15	8.61 <sup>a</sup>	7.26	7.92	7.41	
SAHA	6.95	7.30	6.69 <sup>a</sup>	6.79	7.15	6.21	
<b>1</b>	5.31	5.42	5.76 <sup>a</sup>	4.76	7.31	5.65	
<b>8</b>	6.29	7.00	6.30	6.98	6.37	5.98	

<sup>a</sup> See ref 53.

instead of the hydroxamate. Moreover, the monophosphonic acids **21**, **22**, the (thio)barbiturates **23**–**26**, the nitriles **27**, **28**, and the amidine **29** were synthesized and tested as HDAC inhibitors because such chemical functions are able to chelate metal ions.

Unfortunately, all attempts to obtain non-hydroxamate compounds active as anti-HDAC agents produced only weakly potent (**18**, **25**–**27**, **29**) or totally inactive (**13**–**17**, **19**–**24**, **28**) derivatives. In fact between **1** analogues, the nitrile **27** and the amidine **29** were 7- and 6-fold less potent than their reference compound. With regard to **8** analogues, the hydrazide **18** was 3-fold less effective than **8** in inhibiting the enzyme at fixed dose, and the (thio)barbiturates **25**, **26** were 1000- and 850-fold less active than **8**, respectively.

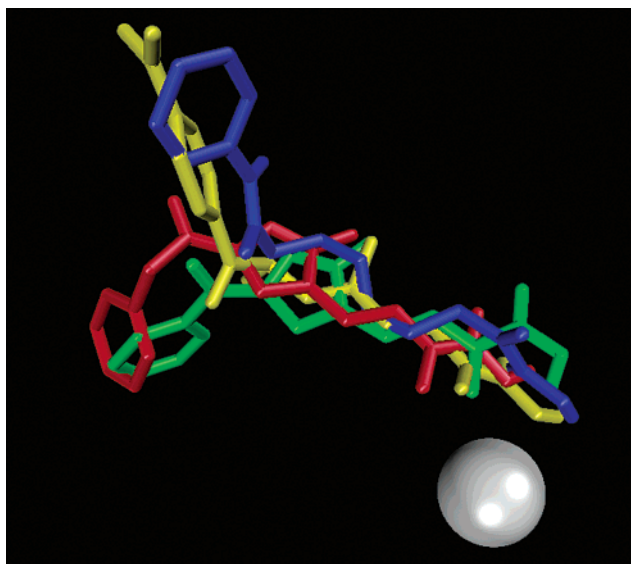
**Docking and Binding Mode Inspection of **1h** into the Modeled HDAC1 Catalytic Core.** Chemical manipulations performed on APHA lead compound **1** highlighted that enzyme inhibiting potency of aroylpyrrole-hydroxyalkylamides is strongly increased by converting the  $C_4$ -benzoyl into  $C_4$ -phenylacetyl moiety at the pyrrole ring, being 3-(1-methyl-4-phenylacetyl-1*H*-2-pyrrolyl)-*N*-hydroxy-2-propenamide **8** 38-fold more active than **1** in in vitro HD2 inhibitory assay (Table 1).

Binding mode analysis of **8** was first investigated using the modeled HDAC1 X-ray structure analogously to that reported for **1**<sup>53</sup> using a semiautomatic dock (SAD) procedure. IC<sub>50</sub> value of **8** against mouse HDAC1 enzyme was determined (Table 2), and its pK<sub>i</sub> was predicted using the in house refined VALIDATE model<sup>57,53</sup> (Table 3). In parallel experiments, docking studies into the HDAC1 catalytic core were also performed on **1**, **8**, TSA, and SAHA structures by the mean of the DOCK 4.0.2<sup>65</sup> and Autodock 3.0.5<sup>66</sup> programs.

Among the minimized ligand/HDAC1 complexes obtained, the most stable ones were those proposed by Autodock (see minimized complex steric energies in Table 4). To compare the four docked molecules (**1**, **8**, TSA, and SAHA), in Figure 2 are reported their binding conformations obtained from the Autodock run. Similarly to that observed for the complexes, also the Autodock conformations showed to be more stable than those obtained with DOCK or SAD procedures (ligand bound steric energies, Table 4).

**Table 4.** Minimized Complex and Ligand Bound Steric Energies (AMBER force field) Relative to **1**, **8**, SAHA, and TSA Obtained by DOCK, Autodock, and SAD Procedures

docking method	<b>1</b>	<b>8</b>	SAHA	TSA
minimized complex steric energy (kJ/mol)				
DOCK	-7174.81	-9077.85	-7369.18	-8909.93
Autodock	-8913.90	-9405.68	-10363.13	-9976.13
SAD	-7828.92	-9142.08	ND <sup>a</sup>	ND
Ligand Bound Steric Energy (kJ/mol)				
DOCK	-12.25	-49.03	-0.53	-48.20
Autodock	-25.11	-53.02	-13.38	-52.74
SAD	-11.50	-54.90	ND	ND

<sup>a</sup> ND, not determined.**Figure 2.** Superimposition of the Autodock docked conformations of **1** (green), **8** (red), TSA (yellow), and SAHA (blue). The gray ball represents the mean position of the zinc ion. HDAC1 pocket is not shown for the sake of clarity

Interestingly, DOCK and Autodock results were in good agreement each other and with those obtained by either the SAD procedure (**1** and **8**) or experimental values (TSA and SAHA) (see Figure 3, and Table C in Supporting Information). The found different binding conformations of **1** (Figure 3A) likely represent three different bound states of the ligand, confirming the low tightness of the HDAC1/**1** complex. On the other hand, for structures endowed with higher activities, the docking methodologies led to almost the same results, reflecting that more stable and unique complexes are achieved for **8**, TSA, and SAHA (Figures 3B–D) (see Experimental Section).

Inspection of **8** binding mode into the HDAC1 catalytic core, compared with that described for **1**,<sup>53</sup> revealed that the enhancement of inhibitory activity can be mainly attributed to the higher flexibility of the pyrrole C<sub>4</sub>-substituent of **8**. Generally, an increase in flexibility is unfavorable, due to the increase in the entropy of binding. Nevertheless, the introduction of a methylene connection between the phenyl and the carbonyl group of the **1** benzoyl moiety disrupts the extended phenyl-CO-pyrrole  $\pi$ -conjugation. As a consequence of this flexibility, **8** fits considerably better than **1** into the HDAC1 pocket, showing a higher average steric fit<sup>57</sup> (**1**<sub>average steric fit</sub> = 1.7; **8**<sub>average steric fit</sub> = 2.0) (Table D in Supporting Information) and providing a more favorable

enthalpy of binding that offsets the slightly more unfavorable entropy (Table 4). Furthermore, this enhanced fitting allows a closer positioning of **8** hydroxamate moiety to the zinc ion (**1**: average CO $\cdots$ Zn = 4.0 Å, average OH $\cdots$ Zn = 4.7 Å; **8**: average CO $\cdots$ Zn = 3.1 Å, average OH $\cdots$ Zn = 3.5 Å).

In Figure 4 the SAD conformation of **8** into the HDAC1 catalytic core is reported. Tyr297 hydroxyl group is placed at hydrogen-bond distance from the **8** hydroxamate moiety (Tyr297-OH $\cdots$ CO<sub>hydroxamate</sub> = 3.25 Å; Tyr297-OH $\cdots$ OH<sub>hydroxamate</sub> = 2.42 Å). Positive  $\pi$ -stacking interactions can be observed between the pyrrolyl-ethylene chain and the Phe141 and Phe198 residues of the site. The pyrrole N<sub>1</sub>-methyl group, contrary to that of **1**,<sup>53</sup> makes favorable interactions with the  $\alpha$ -carbon atom of Gly140 and partially with the Phe141 side chain. This switched position of the **8** N<sub>1</sub>-methyl group with respect to that of **1**<sup>53</sup> allows the molecule to get closer to the catalytic zinc ion. Finally, in the pyrrole C<sub>4</sub>-phenylacetyl portion the ketone points toward the Tyr91 hydroxyl group, probably making a hydrogen bond by the mean of a water molecule (not shown), and the benzene ring points to a hydrophobic region of the enzyme (i.e., Phe200).

#### In Vivo Histone Hyperacetylation Induced by **8**.

To examine whether in vitro HDAC inhibition by **8** correlates with increased acetylation level of core histones in vivo, we treated exponentially growing A20 cells with **8** (40  $\mu$ M) together with TSA (200 nM) and SAHA (11  $\mu$ M) as reference drugs. After isolation of nuclei, the effects on histone acetylation were analyzed by AUT-PAGE (acid-urea-triton polyacrylamide gel electrophoresis) followed by staining with Coomassie brilliant blue R-250. The effect of **1** (800  $\mu$ M) on histone acetylation on mouse A20 cells is also reported for a direct comparison with that of **8**. AUT-PAGE allows separation of individual subspecies of core histones with the different extent of acetylation, because of slower migration rates of the acetylated species. Figure 5 shows that **8** induced the accumulation of highly acetylated histone H4 subspecies (mono- to tetraacetylated) compared to control cells where no toxin was added, with decreases in the most rapidly migrating bands of each histone species.

The effect of **8** on acetylation patterns of histone H4 by an antibody against acetylated H4 peptide was also studied. This antibody recognizes di-, tri-, and tetraacetylated H4, but not nonacetylated H4. In Western Blot experiments isolated histones of Figure 5A were subjected to SDS-PAGE and immunoblotting. Treatment of cells with **8** as well as with **1**, TSA and SAHA led to a highly increased acetylation level of H4 with significant immunoreaction, compared to control histones which show only a faint signal (Figure 5B). Joined to AUT-gel results, these data clearly demonstrate that **8** inhibits HDAC not only in vitro but also in the cells. Moreover, **8** is endowed with higher histone hyperacetylating activity than the APHA prototype **1**, still resulting less potent than TSA and SAHA.

#### Conclusion

We designed and performed structural modifications on 3-(4-benzoyl-1-methyl-1H-2-pyrrolyl)-N-hydroxy-2-propenamide **1**, the representative member of aroyl-

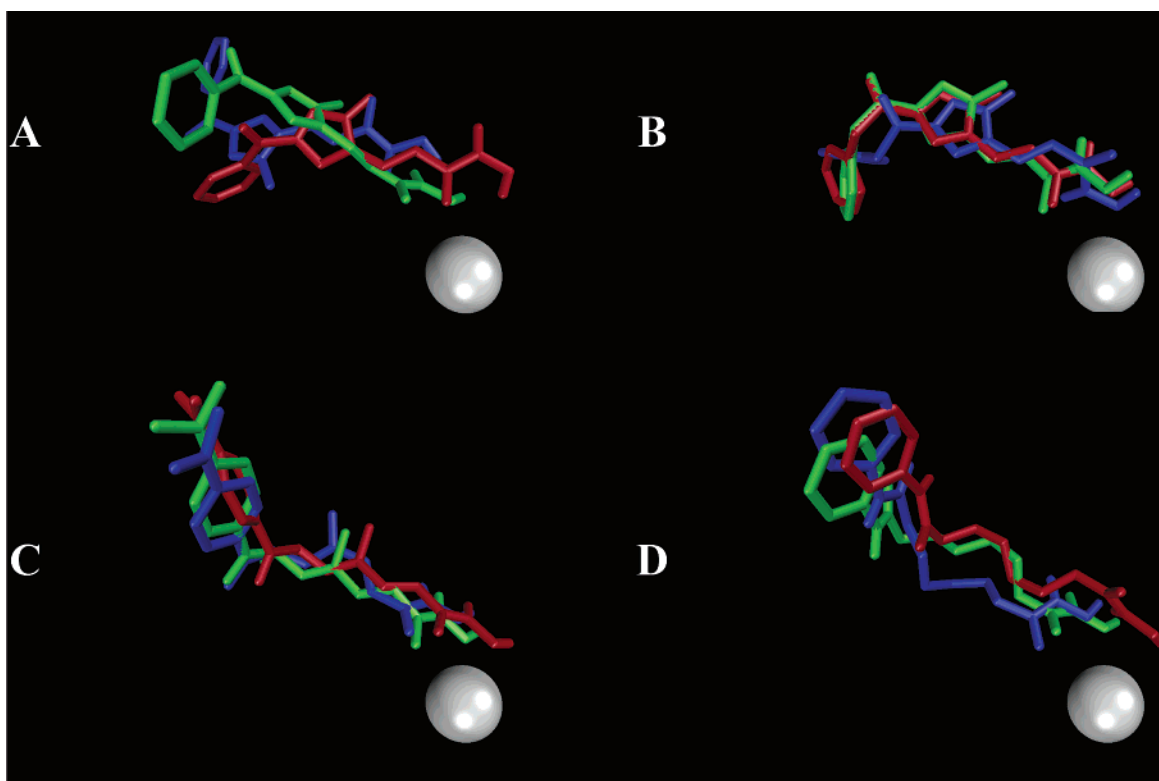


**Figure 3.** Superimposition of the docked conformations of **1** (A), **8** (B), TSA (C), and SAHA (D) obtained from the three docking procedures (see text). The minimized experimental (TSA and SAHA) and the semiautomatic docked (SAD) (**1** and **8**) conformations are in green. Autodock conformations are in red. DOCK conformations are in blue. The gray sphere indicates the Zn ion position into the HDAC1.

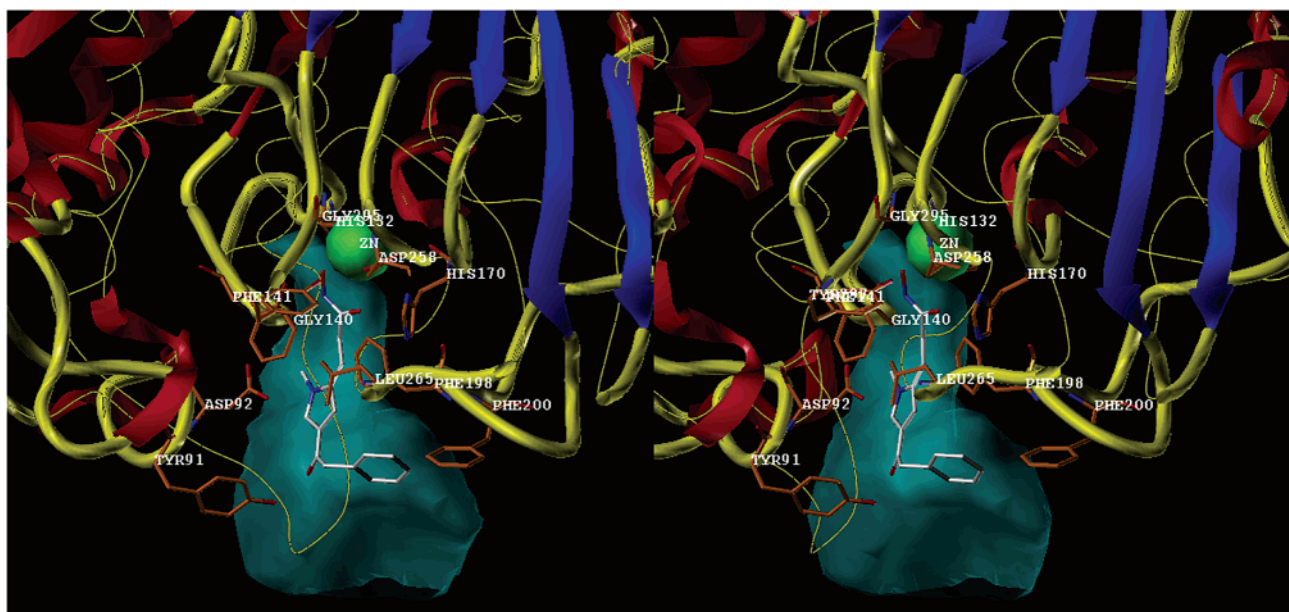


**Figure 4.** Stereoview of the semiautomatic docked conformation of **8** (in white) into the HDAC1 catalytic core. Residues 4 from the ligand are displayed in orange. In transparent cyan is the ligand available volume.

pyrrole-hydroxy-alkylamides (APHAs) recently described by us as a new class of synthetic HDAC inhibitors. In the **1** structure, pyrrole N<sub>1</sub>-substitution with groups larger than methyl decreased HDAC inhibiting activity, and replacement of hydroxamate function with various non-hydroxamate, metal ion-complexing groups yielded low active or totally inactive compounds. On the contrary, proper substitution at the C<sub>4</sub>-position of the pyrrole ring favorably affected enzyme

inhibiting potency, leading to 3-(1-methyl-4-phenylacetyl-1*H*-2-pyrrolyl)-*N*-hydroxy-2-propenamide **8** and 3-[1-methyl-4-(2-phenylethenyl)-1*H*-2-pyrrolyl]-*N*-hydroxy-2-propenamide **9** which were 38- and 3.8-fold more potent than **1** in in vitro anti-HD2 assay, respectively. In comparison with reference drugs, in our enzyme assay **8** showed a 1280-fold higher inhibitory potency than sodium valproate; moreover, it was as active as HC-toxin, and was 14-, 2-, and 10-fold less potent than

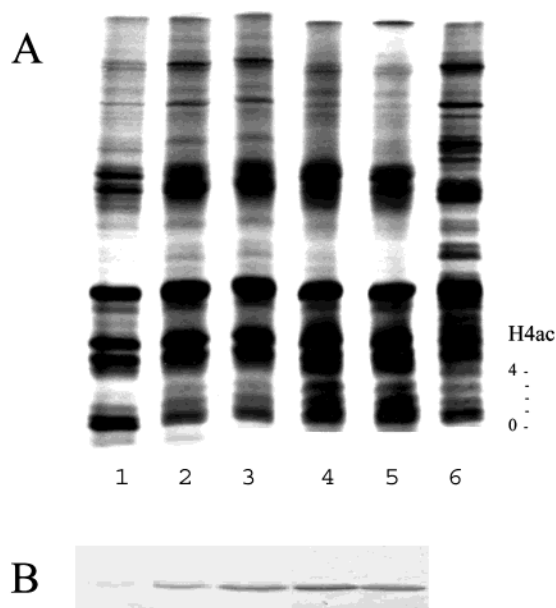


**Figure 5.** Effects of **1**, **8**, TSA, and SAHA on histone acetylation in mouse A20 cells. (A) Analysis of histone hyperacetylation by AUT-PAGE and Coomassie blue staining. Positions of mono- to tetraacetylated H4 subspecies are indicated. (1) control, (2) **1**, (3) **8**, (4) TSA, (5) SAHA, (6) hyperacetylated MELC (murine erythroleukemia cells) histones. (B) Analysis of H4-acetylation by immunoblotting. Position of acetylated H4 is indicated. Data reported in lines 1, 2, 4–6 are the same used in ref 53.

TSA, SAHA, and trapoxin, respectively. Against mouse HDAC1, **8** showed an  $IC_{50} = 0.5 \mu M$ , 10 times more efficient than **1** and 4.5- and 255-fold less potent than SAHA and TSA, respectively. Also in cell-based assay **8** was endowed with higher histone hyperacetylating activity than **1** on mouse A20 cells. Such enhancement of inhibitory activity of **8** with respect to that of **1** can be explained by the binding mode analysis of **8** into the HDAC1 catalytic core. The higher flexibility of the pyrrole  $C_4$ -substituent of **8** accounts for a considerably better fitting into the HDAC1 pocket compared to **1** and allows a closer positioning of **8** hydroxamate moiety to the zinc ion. These findings were supported by extensive docking studies (SAD, DOCK, and Autodock) performed on both APHAs and reference drugs (TSA and SAHA).

We are currently investigating the effect of chemical modifications at the unsaturated chain connecting pyrrole ring with the hydroxamate function in APHA compounds and the capability of **8** to induce antiproliferative effects and terminal cell differentiation.

## Experimental Section

**Chemistry.** Melting points were determined on a Büchi 530 melting point apparatus and are uncorrected. Infrared (IR) spectra (KBr) were recorded on a Perkin-Elmer Spectrum One instrument.  $^1H$  NMR spectra were recorded at 200 MHz on a Bruker AC 200 spectrometer; chemical shifts are reported in  $\delta$  (ppm) units relative to the internal reference tetramethylsilane ( $Me_4Si$ ). All compounds were routinely checked by TLC and  $^1H$  NMR. TLC was performed on aluminum-backed silica gel plates (Merck DC-Alufolien Kieselgel 60 F<sub>254</sub>) with spots visualized by UV light. All solvents were reagent grade and, when necessary, were purified and dried by standard methods. Concentration of solutions after reactions and extractions involved the use of a rotary evaporator operating at a reduced pressure of ca. 20 Torr. Organic solutions were dried over

anhydrous sodium sulfate. Analytical results are within  $\pm 0.40\%$  of the theoretical values. A SAHA sample for biological assays was prepared as previously reported by us.<sup>67</sup> All chemicals were purchased from Aldrich Chimica, Milan (Italy) or Lancaster Synthesis GmbH, Milan (Italy) and were of the highest purity.

**General Procedure for the Synthesis of 4-Aroyl-1H-2-pyrrolicarboxaldehydes 30–40. Example: 4-Benzoyl-1H-pyrrole-2-carboxaldehyde (39).** A 20 mL 1,2-dichloroethane solution of oxalyl chloride (29.7 mmol, 2.6 mL) was added to a cooled ( $0-5^\circ C$ ) solution of *N,N*-dimethylformamide (29.7 mmol, 2.3 mL) in 1,2-dichloroethane (20 mL) over a period of 5–10 min. After being stirred at room temperature for 15 min, the suspension was cooled ( $0-5^\circ C$ ) again and treated with a solution of 1H-pyrrole (29.7 mmol, 2.0 g) in 1,2-dichloroethane (20 mL). The mixture was stirred at room temperature for 15 min and then treated with aluminum trichloride (65.3 mmol, 8.7 g) and benzoyl chloride (29.7 mmol, 3.5 mL). After 3 h, the reaction mixture was poured onto crushed ice (100 g) containing 50% NaOH (20 mL) and stirred for 10 min. The pH of the solution was adjusted to 4 with 37% HCl, the organic layer was separated, and the aqueous one was extracted with chloroform ( $2 \times 20$  mL). The combined organic solutions were washed with water, dried, and evaporated to dryness. The residual oil was purified by column chromatography on silica gel eluting with ethyl acetate:chloroform 1:10. The solid obtained was recrystallized from cyclohexane/benzene to give pure **39**. IR 3220 (NH), 1677 (CHO), 1630 (CO)  $cm^{-1}$ .  $^1H$  NMR ( $CDCl_3$ )  $\delta$  7.45 (m, 4 H, pyrrole  $\beta$ -proton and benzene H-3,4,5), 7.69 (m, 1 H, pyrrole  $\alpha$ -proton), 7.81 (m, 2 H, benzene H-2,6), 9.58 (s, 1 H, CHO), 10.70 (s, 1 H, NH). Anal. ( $C_{12}H_9NO_2$ ) C, H, N.

**General Procedure for the Synthesis of Ethyl 3-(4-Aroyl-1H-2-pyrrolyl)propenoates 41–51. Example: Ethyl 3-(4-Benzoyl-1-phenyl-1H-2-pyrrolyl)propenoate (51).** A suspension of **40** (5.7 mmol, 1.6 g) in absolute ethanol (20 mL) was added in one portion to a mixture of triethyl phosphonoacetate (6.8 mmol, 1.4 mL) and anhydrous potassium carbonate (17.1 mmol, 2.4 g). After being stirred at  $70^\circ C$  for 2 h, the reaction mixture was cooled to room temperature, diluted with water (50 mL), and extracted with ethyl acetate ( $3 \times 30$  mL). The organic layer was washed with water, dried, and evaporated to dryness, and the solid residue was recrystallized to furnish pure **51**. IR 1705 ( $COOC_2H_5$ ), 1633 (CO)  $cm^{-1}$ .  $^1H$  NMR ( $CDCl_3$ )  $\delta$  1.24 (t, 3 H,  $CH_3$ ), 4.13 (q, 2 H,  $CH_2$ ), 6.16 (d, 1 H,  $CH=CHCO$ ), 7.21 (s, 1 H, pyrrole  $\beta$ -proton), 7.31–7.44 (m, 10 H,  $CH=CHCO$ , pyrrole  $\alpha$ -proton, N-benzene H, and CO-benzene H-3,4,5), 7.81 (m, 2 H, CO-benzene H-2,6). Anal. ( $C_{22}H_{19}NO_3$ ) C, H, N.

**Ethyl 3-[4-Benzoyl-1-(1-methylethyl)-1H-2-pyrrolyl]propenoate (52).** A mixture of **50** (19.3 mmol, 5.3 g) and 2-iodopropane (38.6 mmol, 3.9 mL) in *N,N*-dimethylformamide (10 mL) containing anhydrous potassium carbonate (38.6 mmol, 5.3 g) was heated at  $90^\circ C$  while stirring overnight. After being cooled, the mixture was poured onto water (300 mL) and extracted with ethyl acetate ( $3 \times 50$  mL). The organic layer was washed, dried, and evaporated to dryness. The residue was purified by column chromatography on silica gel eluting with ethyl acetate:chloroform 1:10. IR 1705 ( $COOC_2H_5$ ), 1627 (CO)  $cm^{-1}$ .  $^1H$  NMR ( $CDCl_3$ )  $\delta$  1.34 (t, 3 H,  $CH_2CH_3$ ), 1.53 (d, 6 H,  $CH(CH_3)_2$ ), 4.29 (q, 2 H,  $CH_2CH_3$ ), 4.56 (m, 1 H,  $CH(CH_3)_2$ ), 6.31 (d, 1 H,  $CH=CHCO$ ), 7.09 (s, 1 H, pyrrole  $\beta$ -proton), 7.55 (m, 4 H, pyrrole  $\alpha$ -proton and benzene H-3–5), 7.64 (d, 1 H,  $CH=CHCO$ ), 7.84 (m, 2 H, benzene H-2,6). Anal. ( $C_{19}H_{21}NO_3$ ) C, H, N.

**General Procedure for the Synthesis of 3-(4-Aroyl-1H-2-pyrrolyl)propenoic Acids 53–64. Example: 3-[1-Methyl-4-(2-phenylethenyl)-1H-2-pyrrolyl]propenoic Acid (61).** A mixture of **49** (5.7 mmol, 1.8 g), 2 N KOH (22.9 mmol, 11.4 mL), and ethanol (15 mL) was heated at  $70^\circ C$  for 3 h. After being cooled, the solution was poured into water (50 mL) and extracted with ethyl acetate ( $2 \times 20$  mL). To the aqueous layer was added 2 N HCl until the pH was 5, and the precipitate was filtered and recrystallized from benzene giving the pure



compound **61**. IR 3450 (OH), 1705 (COOH), 1640 (CO)  $\text{cm}^{-1}$ .  $^1\text{H NMR}$  (DMSO- $d_6$ )  $\delta$  3.73 (s, 3 H,  $\text{NCH}_3$ ), 6.25 (d, 1 H,  $\text{CH}=\text{CHCOOH}$ ), 7.10–7.56 (m, 8 H, pyrrole  $\beta$ -proton,  $\text{PhCH}=\text{CH}$ , pyrrole  $\alpha$ -proton, and benzene H), 7.77 (m, 1H,  $\text{PhCH}=\text{CH}$ ), 7.99 (m, 1 H,  $\text{CH}=\text{CHCOOH}$ ), 12.10 (s, 1 H, OH). Anal. ( $\text{C}_{17}\text{H}_{15}\text{NO}_3$ ) C, H, N.

**General Procedure for the Synthesis of 3-(4-Aroyl-1-methyl-1*H*-2-pyrrolyl)-*N*-hydroxypropenamides 1–12. Example: 3-(1-Methyl-4-phenylacetyl-1*H*-2-pyrrolyl)-*N*-hydroxypropenamide (**8**).** Ethyl chloroformate (5.0 mmol, 0.5 mL) and triethylamine (5.4 mmol, 0.8 mL) were added to a cooled (0 °C) solution of **60** (4.2 mmol, 1.1 g) in dry THF (10 mL), and the mixture was stirred for 10 min. The solid was filtered off. The filtrate was added to a freshly prepared solution of hydroxylamine, obtained by reaction between hydroxylamine hydrochloride (6.2 mmol, 0.4 g) and KOH (6.2 mmol, 0.35 g), in methanol (10 mL). After being stirred at room temperature for 15 min, the mixture was evaporated under reduced pressure, and the residue was recrystallized from benzene to give the pure compound **8**. IR 3444–3215 (NHOH), 1640 (CONH), 1616 (CO)  $\text{cm}^{-1}$ .  $^1\text{H NMR}$  (DMSO- $d_6$ )  $\delta$  3.74 (s, 3 H,  $\text{NCH}_3$ ), 4.01 (s, 2 H,  $\text{CH}_2$ ), 6.26 (d, 1 H,  $\text{CH}=\text{CHCO}$ ), 6.92 (s, 1 H, pyrrole  $\beta$ -proton), 7.27 (m, 6 H,  $\text{CH}=\text{CHCO}$ , pyrrole  $\alpha$ -proton, and benzene H-2,3,5,6), 7.85 (m, 1 H, benzene H-4), 9.01 (s, 1 H, NH), 10.66 (s, 1 H, OH). Anal. ( $\text{C}_{16}\text{H}_{16}\text{N}_2\text{O}_3$ ) C, H, N.

**General Procedure for the Synthesis of 3-(4-Aroyl-1-methyl-1*H*-2-pyrrolyl)-*N*-methoxypropenamides 13, 17. Example: 3-(1-Methyl-4-phenylacetyl-1*H*-2-pyrrolyl)-*N*-methoxypropenamide (**17**).** To a cooled (0 °C) solution of **60** (1.11 mmol, 0.3 g) in dry THF (10 mL) were added triethylamine (1.45 mmol, 0.21 mL) and ethyl chloroformate (1.33 mmol, 0.13 mL) in succession. After being stirred for 10 min, the mixture was filtered and the filtrate was added to a freshly prepared solution of *O*-methylhydroxylamine, obtained by reaction between *O*-methylhydroxylamine hydrochloride (1.66 mmol, 0.14 g) and KOH (1.66 mmol, 0.1 g), in methanol (5 mL). The resulting mixture was stirred at room temperature for 15 min and then was evaporated under reduced pressure, and the residue was recrystallized from benzene to furnish pure **17**. IR 3190 (NH), 16550 (CONH), 1625 (CO)  $\text{cm}^{-1}$ .  $^1\text{H NMR}$  ( $\text{CDCl}_3$ )  $\delta$  3.71 (s, 3 H,  $\text{NCH}_3$ ), 3.82 (s, 3H,  $\text{OCH}_3$ ), 4.02 (s, 2 H,  $\text{CH}_2$ ), 6.31 (m, 1 H,  $\text{CH}=\text{CHCO}$ ), 7.04 (s, 1 H, pyrrole  $\beta$ -proton), 7.29 (m, 6 H, pyrrole  $\alpha$ -proton and benzene H), 7.65 (d, 1 H,  $\text{CH}=\text{CHCO}$ ), 9.16 (s, 1 H, NH). Anal. ( $\text{C}_{17}\text{H}_{18}\text{N}_2\text{O}_3$ ) C, H, N.

**General Procedure for the Synthesis of 3-(4-Aroyl-1-methyl-1*H*-2-pyrrolyl)propenylhydrazides 14, 18. Example: 3-(1-Methyl-4-phenylacetyl-1*H*-2-pyrrolyl)propenylhydrazide (**18**).** A cooled (0 °C) solution of **60** (1.1 mmol, 0.3 g) in dry THF (10 mL) was treated with triethylamine (1.4 mmol, 0.21 mL) and ethyl chloroformate (1.3 mmol, 0.13 mL) while stirring. After 10 min, the solid was filtered off, and hydrazine hydrate (1.7 mmol, 0.08 mL) was added to the filtrate. The resulting mixture was stirred at room temperature for further 15 min and then was evaporated, and the residue was recrystallized to furnish pure **18**. IR 3200 ( $\text{NHNH}_2$ ), 1650 (CONH), 1620 (CO)  $\text{cm}^{-1}$ .  $^1\text{H NMR}$  ( $\text{CDCl}_3$ )  $\delta$  3.73 (s, 3 H,  $\text{NCH}_3$ ), 4.03 (s, 2 H,  $\text{CH}_2$ ), 6.24 (d, 1 H,  $\text{CH}=\text{CHCO}$ ), 7.02 (s, 1 H, pyrrole  $\beta$ -proton), 7.30 (m, 6 H, pyrrole  $\alpha$ -proton and benzene H), 7.51 (d, 1 H,  $\text{CH}=\text{CHCO}$ ). Anal. ( $\text{C}_{16}\text{H}_{17}\text{N}_3\text{O}_2$ ) C, H, N.

**General Procedure for the Synthesis of 3-(4-Aroyl-1-methyl-1*H*-2-pyrrolyl)-*N*-(2-hydroxyethyl)propenamides 15, 19. Example: 3-(1-Methyl-4-phenylacetyl-1*H*-2-pyrrolyl)-*N*-(2-hydroxyethyl)propenamide (**19**).** A solution of 2-ethanolamine (5.28 mmol, 0.32 mL) and ethyl 3-(1-methyl-4-phenylacetyl-1*H*-2-pyrrolyl)propenoate **48** (1.32 mmol, 0.3 g) was stirred for 2 h at 140 °C. After being cooled, the mixture was poured onto water (100 mL) and extracted with ethyl acetate (3  $\times$  50 mL). The organic layer was washed, dried, and evaporated to dryness to furnish a solid residue (**19**) which was purified by crystallization (benzene/acetonitrile). IR 3280 (NH, OH), 1645 (CONH), 1605 (CO)  $\text{cm}^{-1}$ .  $^1\text{H NMR}$

( $\text{CDCl}_3$ )  $\delta$  1.65 (s, 1 H, OH), 3.58 (m, 2 H,  $\text{CH}_2\text{CH}_2\text{OH}$ ), 3.71 (s, 3 H,  $\text{NCH}_3$ ), 3.84 (m, 2 H,  $\text{CH}_2\text{CH}_2\text{OH}$ ), 4.02 (s, 2 H,  $\text{PhCH}_2$ ), 6.28 (m, 2 H,  $\text{CH}=\text{CHCO}$  and NH), 6.70 (d, 2 H, benzene H-3,5), 7.01 (m, 1 H, pyrrole  $\beta$ -proton), 7.30 (m, 6 H, pyrrole  $\alpha$ -proton and benzene H), 7.53 (d, 1 H,  $\text{CH}=\text{CHCO}$ ). Anal. ( $\text{C}_{18}\text{H}_{20}\text{N}_2\text{O}_3$ ) C, H, N.

**General Procedure for the Synthesis of 3-(4-Aroyl-1-methyl-1*H*-2-pyrrolyl)-2'-hydroxypropenylanilides 16, 20. Example: 3-(1-Methyl-4-phenylacetyl-1*H*-2-pyrrolyl)-2'-hydroxypropenylanilide (**20**).** Triethylamine (2.9 mmol, 0.4 mL) and ethyl chloroformate (2.68 mmol, 0.26 mL) were added to an ice-cooled solution of **60** (2.23 mmol, 0.6 g) in dry THF (10 mL). After being stirred for 10 min, the obtained suspension was filtered, and 2-aminophenol (3.34 mmol, 0.36 g) was added to the filtrate. The resulting mixture was stirred at room temperature for 15 min and then was evaporated under reduced pressure to give crude **20** which was purified by crystallization (benzene/acetonitrile). IR 3120 (NH, OH), 1650 (CONH), 1590 (CO)  $\text{cm}^{-1}$ .  $^1\text{H NMR}$  (DMSO- $d_6$ )  $\delta$  3.50 (s, 3 H,  $\text{NCH}_3$ ), 3.96 (m, 2 H,  $\text{CH}_2$ ), 6.10 (m, 1 H,  $\text{CH}=\text{CHCO}$ ), 6.67 (m, 1 H, pyrrole  $\beta$ -proton), 6.85 (m, 4 H, anilide H-3,4,5 and NH), 7.08 (m, 1 H, anilide H-6), 7.25 (m, 5 H, pyrrole  $\alpha$ -proton and benzene H), 7.74 (m, 1 H,  $\text{CH}=\text{CHCO}$ ), 9.2 (s, 1 H, OH). Anal. ( $\text{C}_{22}\text{H}_{21}\text{N}_2\text{O}_3$ ) C, H, N.

**General Procedure for the Synthesis of Diethyl 2-(4-Aroyl-1-methyl-1*H*-2-pyrrolyl)ethenylphosphonates 65, 66. Example: Diethyl 2-(4-Benzoyl-1-methyl-1*H*-2-pyrrolyl)ethenylphosphonate (**65**).** A suspension of **30** (4.7 mmol, 1.0 g) in absolute ethanol (20 mL) was added in one portion to a mixture of tetraethyl methylenediphosphonate (5.6 mmol, 1.4 mL) and anhydrous potassium carbonate (14.1 mmol, 1.9 g). After being stirred at 70 °C for 2 h, the reaction mixture was cooled to room temperature, poured into water (50 mL), and extracted with ethyl acetate (3  $\times$  25 mL). The combined organic solution was washed with water, dried, and evaporated to dryness. The residual oil was purified by column chromatography on silica gel eluting with ethyl acetate: chloroform 1:1 to furnish pure **65**. IR 1635 (CO), 1240 (P=O), 1025 ( $\text{P}(\text{OC}_2\text{H}_5)_2$ )  $\text{cm}^{-1}$ .  $^1\text{H NMR}$  ( $\text{CDCl}_3$ )  $\delta$  1.27 (t, 6 H,  $\text{CH}_2\text{CH}_3$ ), 3.68 (s, 3 H,  $\text{NCH}_3$ ), 4.04 (q, 4 H,  $\text{CH}_2\text{CH}_3$ ), 5.97 (t, 1 H,  $\text{CH}=\text{CHPO}$ ), 7.01 (s, 1 H, pyrrole  $\beta$ -proton), 7.42 (m, 5 H,  $\text{CH}=\text{CHPO}$ , pyrrole  $\alpha$ -proton, and benzene H-3,4,5), 7.74 (m, 2 H, benzene H-2,6). Anal. ( $\text{C}_{18}\text{H}_{22}\text{NO}_4\text{P}$ ) C, H, N, P.

**General Procedure for the Synthesis of Ethyl 2-(4-Aroyl-1-methyl-1*H*-2-pyrrolyl)ethenylphosphonates 21, 22. Example: Ethyl 2-(1-Methyl-4-phenylacetyl-1*H*-2-pyrrolyl)ethenylphosphonate (**22**).** A mixture of **66** (2.0 mmol, 0.8 g), 2 N KOH (16.1 mmol, 8.1 mL), and ethanol (15 mL) was heated at 70 °C for 3 h. After being cooled, the solution was poured into water (50 mL) and extracted with ethyl acetate (2  $\times$  20 mL). To the aqueous layer was added 2 N HCl until the pH was 5. The precipitate was filtered and recrystallized from benzene/acetonitrile to give pure **22**. IR 3130 (OH), 1626 (CO), 1366 (P=O), 960 ( $\text{POC}_2\text{H}_5$ )  $\text{cm}^{-1}$ .  $^1\text{H NMR}$  ( $\text{CDCl}_3$ )  $\delta$  1.34 (t, 3 H,  $\text{CH}_2\text{CH}_3$ ), 3.58 (s, 3 H,  $\text{NCH}_3$ ), 4.00 (s, 2 H,  $\text{PhCH}_2$ ), 4.10 (q, 2 H,  $\text{CH}_2\text{CH}_3$ ), 6.06 (t, 1 H,  $\text{CH}=\text{CHPO}$ ), 6.07 (s, 1 H, OH overlapped signal), 6.98 (s, 1 H, pyrrole  $\beta$ -proton), 7.29 (m, 7 H,  $\text{CH}=\text{CHPO}$ , pyrrole  $\alpha$ -proton, and benzene H). Anal. ( $\text{C}_{18}\text{H}_{20}\text{PNO}_5$ ) C, H, N, P.

**General Procedure for the Synthesis of 5-[2-(4-Aroyl-1-methyl-1*H*-2-pyrrolyl)ethenyl]-1,2,3,4,5,6-hexahydro-2,4,6-trioxopyrimidines 23, 25, and 5-[2-(4-Aroyl-1-methyl-1*H*-2-pyrrolyl)ethenyl]-4,6-dioxo-1,2,3,4,5,6-hexahydro-2-thioxopyrimidines 24, 26. Example: 5-[2-(4-Benzoyl-1-methyl-1*H*-2-pyrrolyl)ethenyl]-1,2,3,4,5,6-hexahydro-2,4,6-trioxopyrimidine (**23**).** A suspension of barbituric acid (4.4 mmol, 0.56 g) in 15 mL of water was added to a solution of **30** (4.4 mmol, 1.0 g) in ethanol (25 mL), and the mixture was stirred at room temperature for 2 h. The resulting solid was filtered under reduced pressure, collected, and recrystallized to furnish pure **23**. IR 3193 (NH), 1784 (CONH), 1670 (CONH), 1630 (CO)  $\text{cm}^{-1}$ .  $^1\text{H NMR}$  (DMF- $d_7$ )  $\delta$  4.16 (s, 3 H,  $\text{NCH}_3$ ), 7.48 (m, 5 H, pyrrole H and benzene H-3,4,5), 8.44 (d,

2 H, benzene H-2,6), 9.04 (s, 1 H, CH), 11.35 (s, 1 H, NH), 11.45 (s, 1 H, NH). Anal. (C<sub>17</sub>H<sub>13</sub>N<sub>3</sub>O<sub>4</sub>) C, H, N.

**General Procedure for the Synthesis of 3-(4-Aroyl-1-methyl-1H-2-pyrrolyl)propenonitriles 27, 28. Example: 3-(4-Benzoyl-1-methyl-1H-2-pyrrolyl)propenonitrile (27).**

A suspension of **30** (17.01 mmol, 4.47 g) in absolute ethanol (20 mL) was added in one portion to a mixture of diethyl cyanomethylphosphonate (20.41 mmol, 3.3 mL) and anhydrous potassium carbonate (51.03 mmol, 7.05 g). After being stirred at 70 °C for 2 h, the reaction mixture was cooled to room temperature, diluted with water (50 mL), and extracted with ethyl acetate (3 × 25 mL). The organic layer was washed with water, dried, and evaporated to dryness. The residual oil was purified by column chromatography on silica gel eluting with ethyl acetate:chloroform 1:5. Compound **27** was obtained as a solid which was then recrystallized from cyclohexane/benzene. IR 2200 (CN), 1635 (CO) cm<sup>-1</sup>. <sup>1</sup>H NMR (CDCl<sub>3</sub>) δ 3.79 (s, 3 H, NCH<sub>3</sub>), 5.75 (d, 1 H, CH=CHCN), 7.15 (m, 1 H, pyrrole β-proton), 7.31 (d, 1 H, CH=CHCN), 7.42 (m, 1 H, pyrrole α-proton), 7.56 (m, 3 H, benzene H-3,4,5), 7.87 (m, 2 H, benzene H-2,6). Anal. (C<sub>16</sub>H<sub>16</sub>N<sub>2</sub>O) C, H, N.

**3-(4-Benzoyl-1-methyl-1H-2-pyrrolyl)propenylamide (29).** A solution of trimethylaluminum 2.0 M in *n*-hexane (5.8 mmol, 2.9 mL) was slowly added to a 0 °C cooled suspension of ammonium chloride (6.4 mmol, 0.34 g) in toluene (30 mL). After being stirred at room temperature for 2 h, 3-(4-benzoyl-1-methyl-1H-2-pyrrolyl)propenonitrile (**27**) (1.0 g, 3.5 mmol) was added, and the reaction mixture was stirred at 80 °C overnight. After the mixture was cooled at 0 °C, methanol was added to the mixture, and the precipitate was filtered and washed with methanol. The filtrate was evaporated and the residue recrystallized from acetonitrile to afford pure **29**. IR 3400 (NH, NH<sub>2</sub>), 1635 (CO) cm<sup>-1</sup>. <sup>1</sup>H NMR (DMSO-*d*<sub>6</sub>) δ 3.84 (s, 3 H, NCH<sub>3</sub>), 6.21 (d, 1 H, CH=CHC=NH(NH<sub>2</sub>)), 7.79 (m, 7 H, pyrrole H and benzene H), 8.04 (m, 1 H, CH=CHC=NH(NH<sub>2</sub>)), 11.80 (s, 2 H, NH). Anal. (C<sub>16</sub>H<sub>19</sub>N<sub>3</sub>O) C, H, N.

**Biological Assays. HD2 Enzyme Inhibition.** Radioactively labeled chicken core histones were used as the enzyme substrate according to established procedures.<sup>59</sup> The enzyme liberated tritiated acetic acid from the substrate which was quantitated by scintillation counting. IC<sub>50</sub> values are results of triple determinations. Fifty microliters of maize enzyme (at 30 °C) was incubated (30 min) with 10 μL of total [<sup>3</sup>H]acetate-prelabeled chicken reticulocyte histones (1 mg/mL). Reaction was stopped by addition of 36 μL of 1 M HCl/0.4 M acetate and 800 μL of ethyl acetate. After centrifugation (10 000g, 5 min), an aliquot of 600 μL of the upper phase was counted for radioactivity in 3 mL of liquid scintillation cocktail. The compounds were tested in a starting concentration of 40 μM, and active substances were diluted further. Sodium butyrate, sodium valproate, TSA, SAHA,<sup>67</sup> trapoxin, and HC-toxin were used as the reference compounds, and blank solvents were used as negative controls.

**Mouse HDAC1 Enzyme Assay.** For inhibition assay, partially purified HDAC1 from mouse A20 cells (ATCC: TIB-208) (anion exchange chromatography, affinity chromatography (Jesacher and Loidl, unpublished results)) was used as enzyme source. HDAC activity was determined as described<sup>68</sup> using [<sup>3</sup>H]acetate-prelabeled chicken reticulocyte histones as substrate. Fifty microliters of mouse HDAC1 was incubated with different concentrations of compounds for 15 min on ice and 10 μL of total [<sup>3</sup>H]acetate-prelabeled chicken reticulocyte histones (4 mg/mL) were added, resulting in a concentration of 41 μM. The mixture was incubated at 37 °C for 1 h. The reaction was stopped by addition of 50 μL of 1 M HCl/0.4 M acetylacetate and 1 mL ethyl acetate. After centrifugation at 10 000g for 5 min an aliquot of 600 μL of the upper phase was counted for radioactivity in 3 mL of liquid scintillation cocktail.

**In Vivo Histone Hyperacetylation Assay.** Mouse A20 cells (ATCC: TIB-208) were maintained in RPMI 1640 medium at 37 °C and 5% CO<sub>2</sub>. Exponentially growing cells were incubated for 8 h with **8** at final concentration of 40 μM. As references, cells were also treated with TSA (200 nM) and SAHA (11 μM). After incubation, cells were washed and

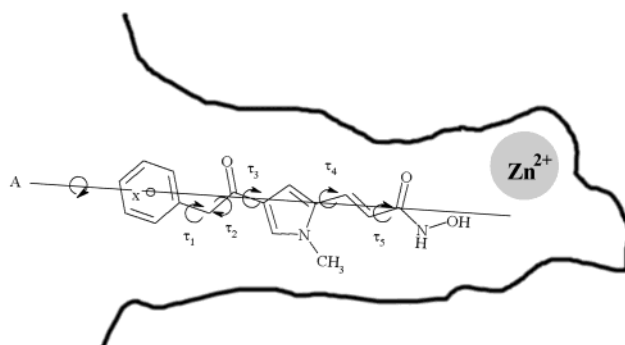


**Figure 6.** Semiautomatic docking procedure generating a family of 748 conformations of **8**. A represents the axis of rotation passing through the center (x) of the benzene ring and the hydroxamic carbon atom.  $\tau_1$ – $\tau_5$  indicate the five rotatable bonds used for the grid searches.

harvested by centrifugation. Isolation of nuclei, extraction of histones, and analysis of histone hyperacetylation by AUT-PAGE (acid-urea-triton polyacrylamide gel electrophoresis) followed by staining with Coomassie brilliant blue R-250 were performed according to standard procedures.<sup>62,69</sup> Hyperacetylation was also investigated by immunoblotting. For this purpose, equal amounts of isolated histones (estimated by laser densitometry) were electrophoresed in precast 14% SDS-polyacrylamide gels and blotted onto nitrocellulose membrane. Membrane strips were incubated with an antibody against acetylated peptide corresponding to the amino acids 2–19 of *Tetrahymena* histone H4 (Upstate Biotechnology). This antibody recognizes highly acetylated histone H4 isoforms (di-, tri-, and tetraacetylated). Immunodetection was performed using secondary antibody alkaline phosphatase conjugates.

**Molecular Modeling Studies.** All molecular modeling calculations and manipulations were performed using the software packages Macromodel 7.1,<sup>70</sup> MOPAC 2000,<sup>71,72</sup> VALIDATE,<sup>57</sup> GOLPE 4.5.12,<sup>73</sup> XlogP 2,<sup>74</sup> Autodock 3.0.5,<sup>65</sup> DOCK 4.0.2,<sup>66</sup> and MIDAS 2.1<sup>75</sup> running on Silicon Graphics O2 R10000, IBM-compatible Intel Pentium IV 1.4 GHz and AMD Athlon 1.9 GHz workstations. For the conformational analysis and for any minimization, the all-atom Amber force field<sup>76,77</sup> was adopted as implemented in the Macromodel package. As previously reported,<sup>53</sup> the crystal structure of TSA extracted from the HDLP/TSA complex filed in the Brookhaven Protein Data Bank<sup>78</sup> (entry code 1c3r) was used. The HDAC1 model was constructed from HDLP by mutating all the residues comprised in a shell of 12 Å from the cocrystallized TSA. Before any docking studies the HDAC1 model was minimized in a vacuum in the presence of TSA to relieve any steric contact introduced by the mutated residue's side chains.

Binding mode of **8** was extensively analyzed by the mean of three different docking procedures. A semiautomatic docking (SAD) was conducted similarly to that reported for **1**. A family of 748 conformations of **8** was generated using the following procedure: the initial conformation of **8** obtained from the reported bound conformation of **1** was arbitrarily rotated by a step of 10° along an axis passing through the center of the benzene ring and the hydroxamic acid carbon atom. Each of the obtained new 36 HDAC1/**8** complexes was submitted to a grid search rotating the five dihedral angles by a step of 30° (Figure 6). By filtering out all of the complexes showing a molecular clashing between **8** and the enzyme pocket, the final conformation family of 748 complexes was achieved. After minimization (Figure 6), the chosen binding conformation of **8** was that associated with the most stable complex (global minimum).

The **8** starting conformation for the docking studies was obtained using molecular dynamics with simulated annealing as implemented in Macromodel version 7.1 and conducted as following: **8** was energy minimized to a low gradient. The nonbonded cutoff distances were set to 20 Å for both van der Waals and electrostatic interactions. An initial random velocity to all atoms corresponding to 300 K was applied. Three

subsequent molecular dynamics runs were then performed. The first was carried out for 10 ps with a 1.5 fs time-step at a constant temperature of 300 K for equilibration purposes. The next molecular dynamic was carried out for 20 ps, during which the system is coupled to a 150 °C thermal bath with a time constant of 5 ps. The time constant represents approximately the half-life for equilibration with the bath; consequently the second molecular dynamic command caused the molecule to slowly cool to approximately 150 K. The third and last dynamic cooled the molecule to 50 K over 20 ps. A final energy minimization was then carried out for 250 iterations using conjugate gradient. The minimizations and the molecular dynamics were in all cases performed in aqueous solution. The atom charges automatically assigned by the batchmin module were retained on **8** for the docking calculations.

For the second docking procedure the program Autodock was used to explore the binding conformation of **8**. For the docking a grid spacing of 0.375 Å and 58 × 52 × 48 number of points were used. The grid was centered on the mass center of the experimental bound TSA coordinates. The GA-LS method was adopted using the default settings. Amber united atom were assigned to the protein using the program ADT (Auto Dock Tools). Autodock generated 100 possible binding conformations for **8** grouped in 32 clusters.

The third docking was performed by the mean of the program DOCK. First, a Connolly surface of each receptor active site was generated by using a 1.4 Å probe radius and further used to generate a set of overlapping spheres that were then clustered according to their spatial distribution. To optimize docking accuracy, spheres located too far away from the known ligand position were eliminated from the finally selected cluster. To compute interaction energies, a 3-D grid of 0.30 Å resolution was centered on TSA experimental bound conformation. The size of the grid box was chosen to enclose all selected spheres using an extra margin of 6 Å. The grid had a size of about 36 × 31 × 33 Å and was composed of about 1 400 000 grid points. Energy scoring grids were obtained by using an all-atom model and a distance-dependent dielectric function ( $\epsilon = 4r$ ) with a 10 Å cutoff. Amber atomic charges were assigned to all protein atoms. The ligand was then docked into the protein active site by matching sphere centers with ligand atoms. A flexible docking (peripheral search and torsion drive) with subsequent minimization was performed as follows: (i) automatic selection and matching of an anchor fragment within a maximum of 10 000 orientations, (ii) iterative growing of the ligand using at least 30 conformations (peripheral seeds) for seeding the next growing stage with assignment of energy-favored torsion angles, (iii) simultaneous relaxation of the base fragments as well as of all peripheral segments and final relaxation of the entire molecule. Orientations/conformations were relaxed in 100 cycles of 100 simplex minimization steps to a convergence of 0.1 kcal/mol. The top 50 solutions corresponding to the best Dock energy scores were then stored in a single multi mol2 file.

Because of neither Autodock nor DOCK are able to perform any energy minimization of the generated complexes, the selection of the binding conformation for **8** was not straightforward by using the first Autodock/DOCK scored conformation. The selection of the binding conformation was performed by an energy-based rescoring of the 32 Autodock cluster representants and the 50 best contact scored DOCK conformations. The program MacroModel was used to minimize the corresponding 32 Autodock and the 50 DOCK HDAC1/**8** complexes. The ligand (**8**) and an 10 Å core of atoms of the pocket were allowed to relax during the minimization. An external fixed shell of 8 Å was also included for the long-range interactions. Because of the presence of a metal Zn ion in the HDAC1 catalytic core and the intrinsic molecular mechanic electrostatic limitation of the AMBER force field, the minimizations were performed applying AM1 charges calculated with the program MOPAC 2000. Furthermore for comparison purpose Autodock and DOCK calculations were also performed on the starting lead compound **1**.

To validate the use of the Autodock and DOCK programs, analogue docking studies were performed on the reference compounds SAHA and TSA. DOCK and Autodock successfully reproduced the experimental binding conformations of the reference drugs with acceptable root-mean-square deviation (RMSD) of atom coordinates. In Table C

(see Supporting Information) are reported the RMSD values of the most stable energy minimized complexes of TSA and SAHA compared with the experimental bound structures (SAHA PDB entry code: 1c3s).<sup>54</sup>

The VALIDATE procedure was used to estimate the binding conformation of the docking studies as previously reported. The partition coefficients were calculated using the program XlogP.

**Acknowledgment.** The authors wish to thank Prof G. Cruciani, University of Perugia, for providing the GOLPE program. This work was supported by grants of "Progetto Finalizzato Ministero della Salute 2002" (A. M.) and the Austrian Science Foundation P13209 (G. B.) and P13620 (P. L.).

**Supporting Information Available:** Chemical and physical data for compounds **1–29**, **37–40**, **48–52**, **60–66**, comparison of docking studies performed on **1**, **8**, TSA, and SAHA (values are the root mean square deviations (RMSDs) for all the atoms), and calculated steric fit values and hydroxamate/Zn distances. This material is available free of charge via the Internet at <http://pubs.acs.org>.

## References

- Wu, J.; Grunstein, M. 25 Years after the nucleosome model: chromatin modifications. *Trends Biochem. Sci.* **2000**, *25*, 619–623.
- Urnov, F. D.; Wolffe, A. Chromatin organization and human disease. *Emerg. Ther. Targets* **2000**, *4*, 665–685.
- Luger, K.; Mader, A. W.; Richmond, R. K.; Sargent, D. F.; Richmond, T. J. Crystal structure of the nucleosome core particle at 2.8 Å resolution. *Nature* **1998**, *389*, 251–260.
- Davie, J. R. Covalent modifications of histones: expression from chromatin templates. *Curr. Opin. Genet. Dev.* **1998**, *8*, 173–178.
- Kouzarides, T. Histone acetylases and deacetylases in cell proliferation. *Curr. Opin. Genet. Dev.* **1999**, *9*, 40–48.
- Strahl, B. D.; Allis, C. D. The language of covalent histone modifications. *Nature* **2000**, *403*, 41–45.
- Grunstein, M. Histone acetylation in chromatin structure and transcription. *Nature* **1997**, *389*, 349–352.
- Pazin, M. J.; Kadonaga, J. T. What is up and down with histone deacetylation and transcription? *Cell* **1997**, *89*, 325–328.
- Glass, C. K.; Rosenfeld, M. G. The coregulator exchange in transcriptional functions of nuclear receptors. *Genes Dev.* **2000**, *14*, 121–141.
- Khochbin, S.; Verdel, A.; Lemerrier, C.; Seigneurin-Berny, D. Functional significance of histone deacetylase diversity. *Curr. Opin. Genet. Dev.* **2001**, *11*, 162–166.
- Giles, R. H.; Peters, D. J.; Breuning, M. H. Conjunction dysfunction: CBP/p300 in human disease. *Trends Genet.* **1998**, *14*, 178–183.
- Gayther, S. A.; Batley, S. J.; Linger, L.; Bannister, A.; Thorpe, K.; Chin, S. F.; Daigo, Y.; Russell, P.; Wilson, A.; Sowter, H. M.; Delhanty, J. D.; Ponder, B. A.; Kouzarides, T.; Caldas, C. Mutations truncating the EP300 acetylase in human cancers. *Nature Genet.* **2000**, *24*, 300–303.
- Goodman, R. H.; Smolik, S. CBP/p300 in cell growth, transformation, and development. *Genes Dev.* **2000**, *14*, 1553–1577.
- Grossman, S. R. p300/CBP/p53 Interactions and regulation of the p53 response. *Eur. J. Biochem.* **2001**, *268*, 2773–2778.
- Lin, R. J.; Sternsdorf, T.; Tini, M.; Evans, R. M. Transcriptional regulation in acute promyelocytic leukemia. *Oncogene* **2001**, *20*, 7204–7215.
- Zelent, A.; Guidez, F.; Melnick, A.; Waxman, S.; Licht, J. D. Translocation of the RAR $\alpha$  gene in acute promyelocytic leukemia. *Oncogene* **2001**, *20*, 7186–7203.
- Pandolfi, P. P. Transcription therapy for cancer. *Oncogene* **2001**, *20*, 3116–3127.
- Grignani, F.; De Matteis, S.; Nervi, C.; Tomassoni, L.; Gelmetti, V.; Cioco, M.; Fanelli, M.; Ruthardt, M.; Ferrara, F. F.; Zamir, I.; Seiser, C.; Grignani, F.; Lazar, M. A.; Minucci, S.; Pelicci, P. G. Fusion proteins of the retinoic acid receptor- $\alpha$  recruit histone deacetylase in promyelocytic leukemia. *Nature* **1998**, *391*, 815–818.

- (19) Lutterbach, B.; Westendorf, J. J.; Linggi, B.; Patten, A.; Moniwa, M.; Davie, J. R.; Huynh, K. D.; Bardwell, V. J.; Lavinsky, R. M.; Rosenfeld, M. G.; Glass, C.; Seto, E.; Hiebert, S. W. ETO, a target of t(8; 21) in acute leukemia, interacts with the N-CoR and mSin3 corepressors. *Mol. Cell. Biol.* **1998**, *18*, 7176–7184.
- (20) Gelmetti, V.; Zhang, J.; Fanelli, M.; Minucci, S.; Pelicci, P. G.; Lazar, M. A. Aberrant recruitment of the nuclear receptor corepressor-histone deacetylase complex by the acute myeloid leukemia fusion partner ETO. *Mol. Cell. Biol.* **1998**, *18*, 7185–7191.
- (21) Wang, J.; Hoshino, T.; Redner, R. L.; Kajigaya, S.; Liu, J. M. ETO, fusion partner in t(8;21) acute myeloid leukemia, represses transcription by interaction with the human N-CoR/mSin3/HDAC1 complex. *Proc. Natl. Acad. Sci. U.S.A.* **1998**, *95*, 10860–10865.
- (22) Ferrara, F. F.; Fazi, F.; Bianchini, A.; Padula, F.; Gelmetti, V.; Minucci, S.; Mancini, M.; Pelicci, P. G.; Lo Coco, F.; Nervi, C. Histone-deacetylase targeted treatment restores retinoic acid signaling and differentiation in acute myeloid leukemia. *Cancer Res.* **2001**, *61*, 2–7.
- (23) Huynh, K. D.; Bardwell, V. J. The BCL-6 POZ domain and other POZ domains interact with the co-repressors N-CoR and SMRT. *Oncogene* **1998**, *17*, 2473–2484.
- (24) Muraoka, M.; Konishi, M.; Kikuchi-Yanoshita, R.; Tanaka, K.; Shitara, N.; Chong, J. M.; Iwama, T.; Miyaki, M. p300 Gene alterations in colorectal and gastric carcinomas. *Oncogene* **1996**, *12*, 1565–1569.
- (25) Weidle, U. H.; Grossmann, A. Inhibition of Histone Deacetylases: a New Strategy to Target Epigenetic Modifications for Anticancer Treatment. *Anticancer Res.* **2000**, *20*, 1471–1486.
- (26) Kramer, O. H.; Göttlicher, M. G.; Heinzel, T. Histone deacetylase as a therapeutic target. *Trends Endocrinol. Metab.* **2001**, *12*, 294–300.
- (27) Marks, P. A.; Richon, V. M.; Breslow, R.; Rifkind, R. A. Histone deacetylase inhibitors as new cancer drugs. *Curr. Opin. Oncol.* **2001**, *13*, 477–483.
- (28) Jung, M. Inhibitors of Histone Deacetylase as New Anticancer Agents. *Curr. Med. Chem.* **2001**, *8*, 1505–1511.
- (29) Johnstone, R. W. Histone-deacetylase inhibitors: novel drugs for the treatment of cancer. *Nature Rev. Drug Discov.* **2002**, *1*, 287–299.
- (30) Yoshida, M.; Kijima, M.; Akita, M.; Beppu, T. Potent and Specific Inhibition of Mammalian Histone Deacetylase both In Vivo and In Vitro by Trichostatin A. *J. Biol. Chem.* **1990**, *265*, 17174–17179.
- (31) Kijima, M.; Yoshida, M.; Suguta, K.; Horinouchi, S.; Beppu, T. Trapoxin, an Antitumor Cyclic Tetrapeptide, Is an Irreversible Inhibitor of Mammalian Histone Deacetylase. *J. Biol. Chem.* **1993**, *268*, 22429–22435.
- (32) Shute, R. E.; Dunlap, B.; Rich, D. H. Analogues of the Cytostatic and Antimitogenic Agents Chlomydocin and HC-Toxin: Synthesis and Biological Activity of Chloromethyl Ketone and Diazomethyl Ketone Functionalized Cyclic Tetrapeptides. *J. Med. Chem.* **1987**, *30*, 71–78.
- (33) Han, J. W.; Ahn, S. H.; Park, S. H.; Wang, S. Y.; Bae, G. U.; Seo, D. W.; Known, H. K.; Hong, S.; Lee, Y. W.; Lee, H. W. Apicidin, a histone deacetylase inhibitor, inhibits proliferation of tumor cells via induction of p21WAF1/Cip1 and gelsolin. *Cancer Res.* **2000**, *60*, 6068–6074.
- (34) Ueda, H.; Nakajima, H.; Hori, Y.; Fujita, T.; Nishimura, M.; Goto, T.; Okuhara, M. FR901228, a novel antitumor bicyclic depsipeptide produced by *Chromobacterium violaceum* No. 968. I. Taxonomy, fermentation, isolation, physicochemical and biological properties, and antitumor activity. *J. Antibiot.* **1994**, *47*, 301–310.
- (35) Kruh, J. Effects of Sodium Butyrate, a New Pharmacological Agent, on Cells in Culture. *Mol. Cell. Biochem.* **1982**, *42*, 65–82.
- (36) Gore, S. D.; Carducci, M. A.; Modifying histones to tame cancer: clinical development of sodium phenylbutyrate and other histone deacetylase inhibitors. *Exp. Opin. Invest. Drugs* **2000**, *9*, 2923–2934.
- (37) Göttlicher, M.; Minucci, S.; Zhu, P.; Kramer, O. H.; Schimpf, A.; Giavara, S.; Sleeman, J. P.; Lo Coco, F.; Nervi, C.; Pelicci, P. G.; Heinzel, T. Valproic acid defines a novel class of HDAC inhibitors inducing differentiation of transformed cells. *EMBO J.* **2001**, *20*, 6969–6978.
- (38) Phiel, C. J.; Zhang, F.; Huang, E. Y.; Guenther, M. G.; Lazar, M. A.; Klein, P. S. Histone deacetylase is a direct target of valproic acid, a potent anticonvulsant, mood stabilizer, and teratogen. *J. Biol. Chem.* **2001**, *276*, 36734–36741.
- (39) Richon, V. M.; Emiliani, S.; Verdin, E.; Webb, Y.; Breslow, R.; Rifkind, R. A.; Marks, P. A. A class of hybrid polar inducers of transformed cell differentiation inhibits histone deacetylases. *Proc. Natl. Acad. Sci. U.S.A.* **1998**, *95*, 3003–3007.
- (40) Jung, M.; Brosch, G.; Kölle, D.; Scherf, H.; Gerhäuser, C.; Loidl, P. Amide Analogues of Trichostatin A as Inhibitors of Histone Deacetylase and Inducers of Terminal Cell Differentiation. *J. Med. Chem.* **1999**, *42*, 4669–4679.
- (41) Remiszewski, S. W.; Sambucetti, L. C.; Atadja, P.; Bair, K. W.; Cornell, W. D.; Green, M. A.; Howell, K. L.; Jung, M.; Known, P.; Trogani, N.; Walker, H. Inhibitors of Human Histone Deacetylase: Synthesis and Enzyme and Cellular Activity of Straight Chain Hydroxamates. *J. Med. Chem.* **2002**, *45*, 753–757.
- (42) Woo, S. H.; Frechette, S.; Khalil, E. A.; Bouchain, G.; Vaisburg, A.; Bernstein, N.; Moradei, O.; Leit, S.; Allan, M.; Fournel, M.; Trachy-Bourget M.-C.; Li, Z.; Besterman, J. M.; Delorme, D. Structurally Simple Trichostatin A-Like Straight Chain Hydroxamates as Potent Histone Deacetylase Inhibitors. *J. Med. Chem.* **2002**, *45*, 2877–2885.
- (43) Uesato, S.; Kitagawa, M.; Nagaoka, Y.; Maeda, T.; Kuwajima, H.; Yamori, T. Novel Histone Deacetylase Inhibitors: N-Hydroxycarboxamides Possessing a Terminal Bicyclic Aryl Group. *Bioorg. Med. Chem. Lett.* **2002**, *12*, 1347–1349.
- (44) Su, G. H.; Sohn, T. A.; Ryu, B.; Kern, S. E. A Novel Histone Deacetylase Inhibitor Identified by High-Throughput Transcriptional Screening of a Compound Library. *Cancer Res.* **2000**, *60*, 3137–3142.
- (45) Kim, Y. B.; Lee, K. H.; Sugita, K.; Yoshida, M.; Horinouchi, S. Oxamflatin is a novel antitumor compound that inhibits mammalian histone deacetylase. *Oncogene* **1999**, *18*, 2461–2470.
- (46) Lavoie, R.; Bouchain, G.; Frechette, S.; Woo, S. H.; Khalil, E. A.; Leit, S.; Fournel, M.; Yan, P. T.; Trachy-Bourget M.-C.; Beaulieu, C.; Li, Z.; Besterman, J. M.; Delorme, D. Design and Synthesis of a Novel Class of Histone Deacetylase Inhibitors. *Bioorg. Med. Chem. Lett.* **2001**, *11*, 2847–2850.
- (47) Furumai, R.; Komatsu, Y.; Nishino, N.; Khochbin, S.; Yoshida, M.; Horinouchi, S. Potent histone deacetylase inhibitors built from trichostatin A and cyclic tetrapeptide antibiotics including trapoxin. *Proc. Natl. Acad. Sci. U.S.A.* **2001**, *98*, 87–92.
- (48) Komatsu, Y.; Tomizaki, K.; Tsukamoto, M.; Kato, T.; Nishino, N.; Sato, S.; Yamori, T.; Tsuruo, T.; Furumai, R.; Yoshida, M.; Horinouchi, S.; Hayashi, H. Cyclic Hydroxamic acid-containing Peptide 31, a Potent Synthetic Histone Deacetylase Inhibitor with Antitumor Activity. *Cancer Res.* **2001**, *61*, 4459–4466.
- (49) Suzuki, T.; Ando, T.; Tsuchiya K.; Fukazawa, N.; Saito, A.; Mariko, Y.; Yamashita, T.; Nakanishi, O. Synthesis and Histone Deacetylase Inhibitory Activity of New Benzamide Derivatives. *J. Med. Chem.* **1999**, *42*, 3001–3003.
- (50) Saito, A.; Yamashita, T.; Mariko, Y.; Nosaka, Y.; Tsuchiya, K.; Ando, T.; Suzuki, T.; Tsuruo, T.; Nakanishi, O. A synthetic inhibitor of histone deacetylase, MS-27–275, with marked in vivo antitumor activity against human tumors. *Proc. Natl. Acad. Sci. U.S.A.* **1999**, *96*, 4592–4597.
- (51) Vigushin, D. M.; Coombes, R. C. Histone deacetylase inhibitors in cancer treatment. *Anti-Cancer Drugs* **2001**, *13*, 1–13.
- (52) Massa, S.; Mai, A.; Sbardella, G.; Esposito, M.; Ragno, R.; Loidl, P.; Brosch, G. 3-(4-Aroyl-1H-pyrrol-2-yl)-N-hydroxy-2-propenamides, a New Class of Synthetic Histone Deacetylase Inhibitors. *J. Med. Chem.* **2001**, *44*, 2069–2072.
- (53) Mai, A.; Massa, S.; Ragno, R.; Esposito, M.; Sbardella, G.; Nocca, G.; Scatena, R.; Jesacher, F.; Loidl, P.; Brosch, G. Binding Mode Analysis of 3-(4-Benzoyl-1-methyl-1H-2-pyrrolyl)-N-hydroxy-2-propenamide: A New Synthetic Histone Deacetylase Inhibitor Inducing Histone Hyperacetylation, Growth Inhibition, and Terminal Cell Differentiation. *J. Med. Chem.* **2002**, *45*, 1778–1784.
- (54) Finnin, M. S.; Donigian, J. R.; Cohen, A.; Richon, V. M.; Rifkind, R. A.; Marks, P. A.; Breslow, R.; Pavletich, N. P. Structures of a histone deacetylase homologue bound to the TSA and SAHA inhibitors. *Nature* **1999**, *401*, 188–193.
- (55) Massa, S.; Artico, M.; Corelli, F.; Mai, A.; Di Santo, R.; Cortes, S.; Marongiu, M. E.; Pani, A.; La Colla, P. Synthesis and Antimicrobial and Cytotoxic Activities of Pyrrole-Containing Analogues of Trichostatin A. *J. Med. Chem.* **1990**, *33*, 2845–2849.
- (56) Corelli, F.; Massa, S.; Stefanich, G.; Mai, A.; Artico, M.; Panico, S.; Simonetti, N. Ricerche su composti antibatterici ed antifungini. Nota VIII – Sintesi ed attività antifungina di derivati pirrolici correlati con la tricostatina A. (Researches on antibacterial and antifungal agents. VIII. Synthesis and antifungal activity of trichostatin A-related pyrrole derivatives.) *Farm., Ed. Sci.* **1987**, *42*, 893–903.
- (57) Head, R. D.; Smythe, M. L.; Oprea, T. I.; Waller, C. L.; Green, S. M.; Marshall, G. R. VALIDATE: A New Method for the Receptor-Based Prediction of Binding Affinities of Novel Ligands. *J. Am. Chem. Soc.* **1996**, *118*, 3959–3969.
- (58) Garigipati, R. S. An efficient conversion of nitriles to amidines. *Tetrahedron Lett.* **1990**, *31*, 1969–1972.

- (59) Lechner, T.; Lusser, A.; Brosch, G.; Eberharter, A.; Goralik-Schramel, M.; Loidl, P. A comparative study of histone deacetylases of plant, fungal and vertebrate cells. *Biochim. Biophys. Acta* **1996**, *1296*, 181–188.
- (60) HD2-activity was extensively purified by anion exchange chromatography (Q-Sepharose), affinity chromatography (Heparin-Sepharose, Histone-Agarose), and size exclusion chromatography (Superdex S200) as described elsewhere.<sup>60,61</sup>
- (61) Brosch, G.; Lusser, A.; Goralik-Schramel, M.; Loidl, P. Purification and characterization of a high molecular weight histone deacetylase complex (HD2) of maize embryos. *Biochemistry* **1996**, *35*, 15907–15914.
- (62) Kölle, D.; Brosch, G.; Lechner, T.; Lusser, A.; Loidl, P. Biochemical methods for analysis of histone deacetylases. *Methods* **1998**, *15*, 323–331.
- (63) Kölle, D.; Brosch, G.; Lechner, T.; Pipal, A.; Helliger, W.; Taplick, J.; Loidl, P. Different types of maize histone deacetylases are distinguished by a highly complex substrate and site specificity. *Biochemistry* **1999**, *38*, 6769–6773.
- (64) Brosch, G.; Ransom, R.; Lechner, T.; Walton, J.; Loidl, P. Inhibition of maize histone deacetylases by HC toxin, the host-selective toxin of *Cochliobolus carbonum*. *Plant Cell* **1995**, *33*, 1941–1950.
- (65) Oshiro, C. M.; Kuntz, I. D.; Dixon, J. S. Flexible ligand docking using a genetic algorithm. *J. Comput. Aided Mol. Des.* **1995**, *9*, 113–130.
- (66) Goodsell, D. S.; Morris, G. M.; Olson, A. J. Automated docking of flexible ligands: applications of AutoDock. *J. Mol. Recognit.* **1996**, *9*, 1–5.
- (67) Mai, A.; Esposito, M.; Sbardella, G.; Massa, S. A new facile and expeditious synthesis of N-hydroxy-N'-phenyloctanediamide, a potent inducer of terminal cytodifferentiation. *Org. Prep. Proced. Int.* **2001**, *33*, 391–394.
- (68) Rowley, P. T.; Ohlsson-Wilhelm, B. M.; Farley, B. A.; La Bella, S. Inducers of erythroid differentiation in K562 human leukemia cells. *Exp. Hemat.* **1981**, *9*, 32–37.
- (69) Alfageme, C. R.; Zweidler, A.; Mahowald, A.; Cohen, L. H. Histones of *Drosophila* embryos. Electrophoretic isolation and structural studies. *J. Biol. Chem.* **1974**, *249*, 3729–3736.
- (70) Mohamadi, F.; Richards, N. G. J.; Guida, W. C.; Liskamp, R.; Lipton, M.; Caufield, C.; Chang, G.; Hendrickson, T.; Still, W. C. MACROMODEL – an integrated software system for modeling organic and bioorganic molecules using molecular mechanics. *J. Comput. Chem.* **1990**, *11*, 440–467.
- (71) Stewart, J. J. MOPAC: a semiempirical molecular orbital program. *J. Comput. Aided Mol. Des.* **1990**, *4*, 1–105.
- (72) *MOPAC 2000.00 Manual*; Stewart, J. J. P., Ed; Fujitsu Limited: Tokyo, Japan, 1999.
- (73) *GOLPE*. Multivariate Infometric Analysis Srl.: Viale dei Castagni 16, Perugia, Italy, 1999.
- (74) Wang, R.; Fu, Y.; Lai, L. A New Atom-Additive Method for Calculating Partition Coefficients. *J. Chem. Inf. Comput. Sci.* **1997**, *37*, 615–621.
- (75) Ferrin, T. E.; Huang, C. C.; Jarvis, L. E.; Langridge, R. The MIDAS Display System. *J. Mol. Graphics* **1988**, *6*, 13–27.
- (76) Pearlman, D. A.; Case, D. A.; Caldwell, J. W.; Ross, W. S.; Cheatham T. E., III.; Debolt, S.; Ferguson, D. M.; Seibel, G. L.; Kollman, P. A. AMBER, a Package of Computer Programs for Applying Molecular Mechanics, Normal-Mode Analysis, Molecular Dynamics and Free Energy Calculations to Simulate the Structural and Energetic Properties of Molecules. *Comput. Phys. Commun.* **1995**, *91*, 1–41.
- (77) Pearlman, D. A.; Case, D. A.; Caldwell, J. W.; Ross, W. S.; Cheatham, T. E., III; Ferguson, D. M.; Seibel, G. L.; Singh, U. C.; Weiner, P. K.; Kollman, P. A. AMBER 4.1; Department of Pharmaceutical Chemistry, University of California: San Francisco, CA, 1995.
- (78) Berman, H. M.; Westbrook, J.; Feng, Z.; Gilliland, G.; Bhat, G. N.; Weissig, H.; Shindyalov, I. N.; Bourne, P. E. The Protein Data Bank. *Nucl. Acids Res.* **2000**, *28*, 235–242.

JM021070E